New evidence of glacier advances during Lateglacial Interstadial deciphered from facies evolution in proglacial lacustrine basins of the Maurienne Valley, French Alps.

Thibault Roattino, Jean-François Buoncristiani, Christian Crouzet, Riccardo Vassallo

Quaternary Science Advances 16 (2024) 100242

Contents lists available at ScienceDirect

Quaternary Science Advances

journal homepage: www.sciencedirect.com/journal/quaternary-science-advances

New evidence of glacier advances during Lateglacial Interstadial deciphered from facies evolution in proglacial lacustrine basins of the Maurienne Valley, French Alps

Thibault Roattino [a,*], Jean-François Buoncristiani [b], Christian Crouzet [a], Riccardo Vassallo [a]

[a] Univ. Savoie Mont Blanc, Univ. Grenoble Alpes, CNRS, IRD, Univ. Gustave Eiffel, ISTerre, 73000, Chambéry, France
[b] Biogéosciences, UMR/CNRS 6282, Université de Bourgogne, 6 Bd Gabriel, 21000, Dijon, France

ARTICLE INFO

Keywords:
Alps
Glacier
Sedimentology
Proglacial lake
Bølling-Allerød Interstadial

ABSTRACT

Sedimentological analysis of glaciolacustrine deposit in the French Alps provides an opportunity to elucidate poorly understood glacier fluctuations during the Lateglacial Interstadial. This study focuses on two proglacial lacustrine basins in the Maurienne Valley, Le Verney and Lanslebourg, recording sediment deposition during the Lateglacial. Sedimentological and soft sediment deformation analyses were conducted on these glaciolacustrine sedimentary deposits to constrain the dynamic of the Arc glacier. At Le Verney, the sedimentary succession records the deposition of a proglacial subaquatic fan under supercritical conditions, transitioning to a Gilbert delta-type sedimentation, indicating glacier retreat. Fluid overpressure, shear deformations, and compressional stresses found within Gilbert delta-type sediment marks a subsequent glacier advance. In the Lanslebourg basin, sedimentary deposits display supercritical and subcritical conditions, separated by deposition under a hydraulic jump characteristic of ice contact delta. In this area, glacier advance is recorded by a more proximal condition toward the top of the sedimentary succession, along with a transition to a subglacial condition. These findings reveal glacier advances during the Bølling-Allerød Interstadial, providing the first evidence of glacier re-advances in the French northern Alps during this warming period. This result highlights the complex interactions between local climate, glacier dynamics, and topography.

1. Introduction

On the scale of millennial to centennial climatic cycles, the advances and retreats of mountain glaciers can serve as a proxy for continental paleoclimatic reconstructions (Kerschner and Ivy-Ochs, 2008; Davis et al., 2009; Mackintosh et al., 2017). However, the response of glaciers to century-scale climatic fluctuations does not always result in the formation of distinct glacial morphologies. Furthermore, the inherent uncertainties in the dating techniques employed to determine the ages of these morphologies (e.g., cosmogenic radionuclides exposure ages) often exceed the duration of these transient events (Braumann et al., 2022).

Lateglacial warming is punctuated by cold events on millennial to pluricentennial climatic scales, as evidenced by the isotope stratigraphy of synchronized Greenland ice core records (Rasmussen et al., 2014). Two millennia-long cold events have been identified in Greenland ice cores, the Oldest Dryas (GS-2.1a: 17.5–14.6 ka b2k) and the Younger Dryas (GS-1: 12.9–11.7 ka b2k) characterized by an abrupt decrease of the temperature (Alley et al., 1993; Denton et al., 2010; Rasmussen et al., 2014). The Bølling-Allerød Interstadial (GI-1: 14.6–12.9 ka b2k) represents the most prominent warm event during the last deglaciation in the Northern hemisphere (Hoek, 2009). Its existence was initially inferred from flora assemblage that was reconstructed by the analysis of pollen and plant remains in Denmark (Hartz and Milthers, 1901; Iversen, 1942, 1954); deep lake ostracods oxygen isotope in Ammersee (Von Grafenstein et al., 1999). Lateglacial timing of events correlation (Brauer et al., 2000b; Van Raden et al., 2013) show that the Bølling-Allerød began with an abrupt warming period interrupted by pluricentennial-long cold events: the Older Dryas (GI-1d: 13,908–14,044 b2k) and the intra-Allerød cold events (GI-1b: 12,989–13,274 b2k).

The Younger Dryas glacier readvance in the Alps was extensively documented through the dating of moraines in various locations including Austria (Kerschner, 1980; Ivy-Ochs et al., 2006, 2009; Moran et al., 2016), Italy (Ivy-Ochs et al., 2008; Federici et al., 2008, 2017;

* Corresponding author.
E-mail address: thibault.roattino@univ-smb.fr (T. Roattino).

https://doi.org/10.1016/j.qsa.2024.100242
Received 16 April 2024; Received in revised form 10 September 2024; Accepted 15 September 2024
Available online 19 September 2024

Baroni et al., 2014, 2017; Reitner et al., 2016; Spagnolo and Ribolini, 2019), Switzerland (Ivy-Ochs et al., 2009; Boxleitner et al., 2019), and France (Jaillet and Ballandras, 1999; Darnault et al., 2011; Cossart et al., 2012; Chenet et al., 2016; Protin et al., 2019).

While some results argue that the onset of warming during the Bølling-Allerød Interstadial triggered a phase of glacier recession in the Alps, possibly resulting in significantly smaller glacier extents compared to the Younger Dryas period (Ivy-Ochs et al., 2023), others present evidence suggesting contrary viewpoints. For instance, in the Tatra Mountains, moraines have been dated to 13.4 ± 0.5 ka with ^{10}Be (Engel et al., 2017). Similarly, in the Central Pyrenees, specifically in the Ruda Valley, glaciers underwent two distinct phases of advance or stillstand,

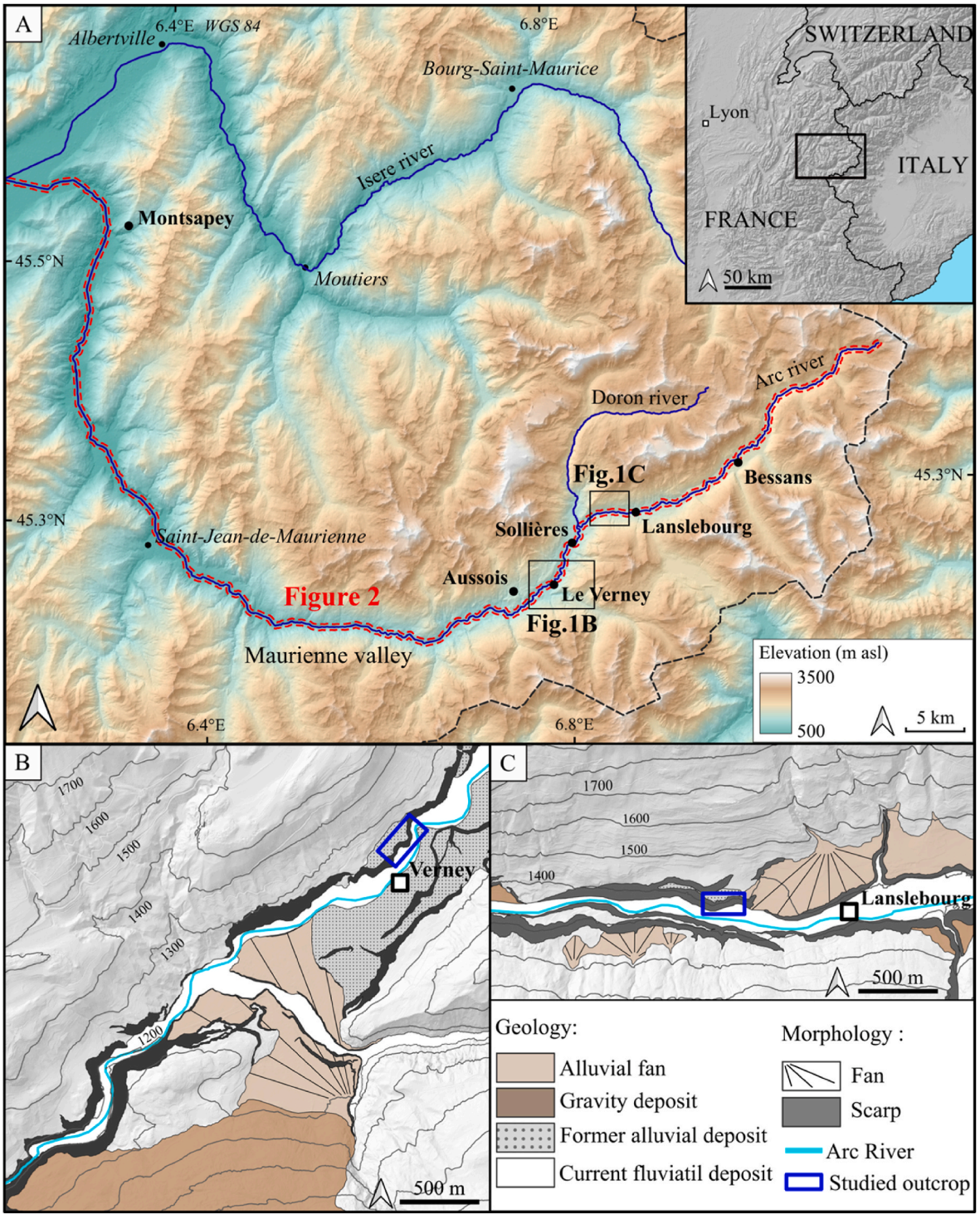

Fig. 1. (A) Map of the French Alps showing the altitude (DEM ALOS World 3D - 30m AW3D30) of the regions in the study area (colored according to altitude) with the main location used in this study, mainly the Arc valley and the Doron valley. The Maurienne valley corresponds to the path of the Arc river and extends over more than 120 km. The red dashed line box shows the location of the topographic river profile shown in Fig. 2 (B) Quaternary geological and geomorphological map of the Le Verney basin. (C) Quaternary geological and geomorphological map of the Lanslebourg basin. (For interpretation of the references to color in this figure legend, the reader is referred to the Web version of this article.)

resulting in moraine formation at 13.5 and 13.0 ka (Fernandes et al., 2022). Moreover, indirectly dated degraded moraines in Austria (Ivy-Ochs, 2015) and exposure dating on glacial boulders in Italy (Serra et al., 2022) provide corroborative evidence indicating that glaciers might have been larger during the Older Dryas and the Intra-Allerød Cold Event.

However, recording climatic variations on a puricentennial scale during the Bølling-Allerød in terrestrial alpine glacial moraine deposits remains highly challenging. Rapid glacial advances during this period may not necessarily result in moraines formation (Rowan et al., 2022), or these deposits may undergo erosion due to multiple glacier advances (Gibbons et al., 1984). An alternative approach could involve examining of the sedimentology and deformation processes from proglacial deposits (Ashley, 1995; Lang et al., 2021 and references therein), which provides valuable insights into past climatic variations. Through this approach, it becomes possible to reconstruct glacial dynamics that are not recorded in glacial geomorphologies. This approach has been widely employed across various contexts, facilitating the reconstruction of glacial dynamics for Pleistocene glaciations in Canada (Tracy and Brennand, 2000), Norway (Lonne et al., 2001), Alaska (Bennett et al., 2002), and Iceland (Ravier et al., 2015).

After the Last Glacial Maximum (LGM; 26.5-19 ka; Clark et al., 2009), the glaciers in the Western French Alps retreated from the foreland (Roattino et al., 2022) and withdrew into the alpine valleys. In this study, our focus is on the Maurienne Valley, which was occupied by the Arc glacier (Kilian and Révil, 1917; Hugonin, 1988) during the Lateglacial period (19.0-11.7 ka b2k; Rasmussen et al., 2014). In this area, two proglacial lacustrine basins are outcropping in Le Verney and Lanslebourg (Kilian and Révil, 1917; Hugonin, 1988; Debelmas, 1989; Fudral et al., 1994; Marnézy, 1999; Champagnac et al., 2006). In these deposits, sedimentological, stratigraphical and deformational criteria are used to interpret the glacier dynamics. The objective of these analyses is to provide new insights into the glacier dynamics during the Lateglacial period in the French Alps.

2. Geological and chronological setting

2.1. Geological setting

The study area is located in the French Alps (Fig. 1A) in the Maurienne Valley where the Arc river flows. The studied outcrops are located in two quarries near Le Verney and Lanslebourg (Fig. 1A). The sediments studied at Le Verney and Lanslebourg provide evidence of the sedimentary infilling of two proglacial lakes resulting from glacial erosion. Geological bedrock in the study area is located at the junction of the briançonnaise and piemontaise alpine units. The first one is mainly composed of Triassic quartzite and carbonates. The second one consists of the "Schistes lustrés" which are metamorphosed under blueschist facies and have experienced ductile deformation. A thick layer of evaporites underlines the contact between the two major units (Fudral, 1998).

The first glaciolacustrine deposit is located at Le Verney and corresponds, based on its position, to a former proglacial lake developed at the front of a glacier resulting from the confluence of the Arc glacier and the Doron glacier (Hugonin, 1988). The bedrock of Le Verney basin is composed of Triassic dolomite and evaporites (Debelmas, 1989). A glacial knickpoints composed by Triassic quartzite, dolomite and schists, at an altitude of ~1250 m, is at the origin of proglacial lake allowing deposition of deltaic sediments in the Le Verney basin (Hugonin, 1988). This basin exhibits an elongated shape about 5 km long for 400–600 m width. It is oriented NE-SW at an altitude varying from 1200 to 1270 m asl. At Le Verney, the proglacial deposits are overlain by fluvial alluvium deposits with a flat topography. This terrace is at the same elevation as the glacial knickpoints. Le Verney basin includes also alluvial fans and gravity deposits (Debelmas, 1989). In this area, the Arc River has incised proglacial and post-deltaic deposits (Fig. 1B) (Hugonin, 1988).

The second proglacial lake is located in the Lanslebourg basin (Fig. 1C), upstream from Le Verney, and is thought to result from a glacial advance of the Arc glacier (Hugonin, 1988). Its substratum is composed by Mesozoic schists (Fudral et al., 1994). At Sollière, fluvial or glaciofluvial deposits are overlain by a diamicton. The lacking of ophiolites and orthogneiss in these glacial sediments indicates that they were transported by the Doron glacier rather than the Arc glacier (Hugonin, 1988). The Sollières outcrop demonstrates that the Doron glacier serve as a glacial dam located between Le Verney and Lanslebourg basin (Fig. 1A). This glacial dam leads to the formation of the Lanslebourg paleolake, which was fed by meltwater from the Arc glacier and allowing deposition of proglacial sediments (Hugonin, 1988). The Lanslebourg basin forms an elongated shape of 7 km long and 100–500 m width, oriented E-W at an altitude varying from 1350 to 1450 m asl. The deltaic and fine lacustrine sediments are overlain by alluvial deposits, interpreted either as being formed in glaciolacustrine or fluvioglacial environments (Fudral et al., 1994; Marnézy, 1999) or as a part of alluvial fan deposit (Hugonin, 1988) associated with subhorizontal topography. This terrace is situated at 1415 m asl, approximately 15–20 m higher than the elevation of the glacial knickpoints. This observation further supports the hypothesis of a glacial dam. Subsequently, all these deposits are then incised by the Arc river (Fig. 1A) (Hugonin, 1988).

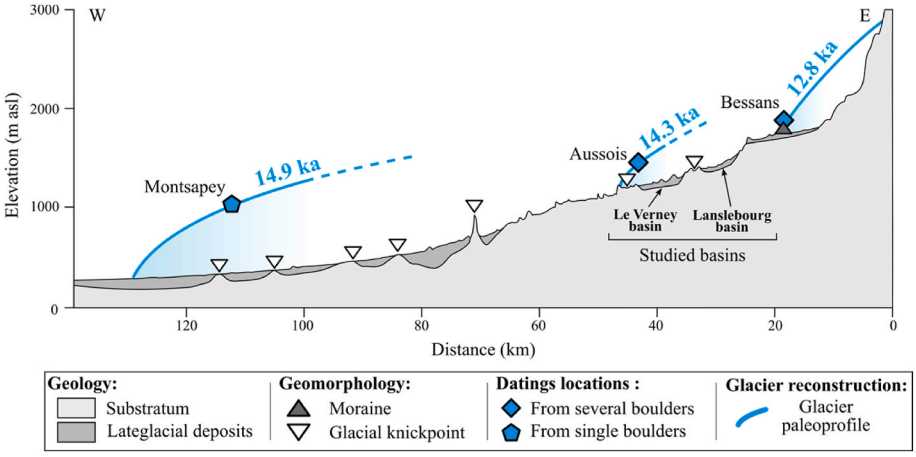

Fig. 2. Topographic river profile of the Maurienne Valley displaying the location of the Lateglacial deposits and the supposed bedrock topography (Hugonin, 1988; Crouzet et al., 1999). Geomorphological features such as glacial knickpoints and moraine are represented. Dated ^{10}Be cosmogenic boulders at Montsapey, Aussois and Bessans (Nicoud et al., 2009; Prud'homme et al., 2020) and their respective glacier paleoprofiles are also shown. Position of the profile is given in Fig. 1A.

2.2. Chronological setting

The chronology of glaciolacustrine deposits in the upper Maurienne Valley, between Le Verney and Lanslebourg, may be constrained using cosmogenic age data (^{10}Be) obtained from erratic boulders. These ^{10}Be exposure ages are given in Prud'homme et al. (2020) from boulders at Montsapey and Aussois and in Nicoud et al. (2009) from boulders sampled at Bessans (Fig. 2). Sample ages from these studies will be used throughout the present paper. Exposure ages have been recalculated and harmonized using the updated parameters for production rates in the Cosmic Ray Exposure Program (CREP, univ-lorraine.fr) (Martin et al., 2017). We used the scaled production rate based on the Chironico landslide production rate calibration (4.16 ± 0.10 at/g/yr; Claude et al., 2014) with the production rate scaling scheme of LSD model (Lifton et al., 2014). ^{10}Be ages in this valley are associated with two types of landforms: glacial polished surfaces and erratic boulders. Erratic boulders were sampled throughout all dated sites which is not the case for glacial polished surfaces. Moreover, several studies showed that ages determined on erratic boulders are generally more reliable because they are less sensitive to the effect of temporal burial by sediments or snow (Briner et al., 2005; Heyman et al., 2011, 2016). For these reasons, and in order to have a set of a homogeneous type of samples at sites located downstream and upstream the study area, we therefore chose to use only the ages on erratic boulders. Ages for sites with multiple boulders (Aussois, Bessans) have been obtained by calculating a weighted mean of samples exposure ages with an error-weighted uncertainty. All sites show evidence of good preservation of landforms from denudation and degradation since the glacial retreat. All boulders are characterized by a different lithology with respect to the underlying or surrounding bedrock, evidence of a significant glacial transport.

At Montsapey (Fig. 2), the only available boulder is located at 1005 m asl, in the vicinity of a polished bedrock surface on a flatter zone along the hillslope (Prud'homme et al., 2020). It yields a re-calculated exposure age of 14.9 ± 1.8 ka.

At Aussois (Fig. 2), three boulders are located close to each other at 1470 m asl above a large glacial polished surface, indicating a simultaneous abandonment by the glacier (Prud'homme et al., 2020). They are dated respectively at 14.25 ± 0.64 ka, 15.10 ± 1.03 ka, and 13.86 ± 0.75 ka. The weighted mean yields an exposure age for Aussois site of 14.27 ± 0.44 ka.

At Bessans (Fig. 2), four boulders are located on a well-preserved frontal morainic ridge at 1740 m asl (Nicoud et al., 2009). This moraine indicates a glacial advance following a retreat phase. Consequently, the dating of these boulders, unlike that of previous sites, is associated with a glacier advance. Recalculated exposure ages for these boulders are 13.67 ± 1.00 ka, 12.20 ± 0.56 ka, 12.37 ± 1.03 ka, and 13.23 ± 0.64 ka. The weighted mean yields an exposure age for Bessans moraine at 12.75 ± 0.36 ka, corresponding to the Younger Dryas.

Following Prud'homme et al. (2020), all these ages should be considered as maximum ones because of potential inherited ^{10}Be concentrations. However, both chrono-stratigraphical coherence along the valley and low scattering at each site are compatible with a simple exposure history for these boulders. We therefore consider that these exposure ages cannot exceed significantly the real abandonment ages and may be used to date the deglaciation in upper Maurienne Valley.

Using ^{10}Be cosmogenic age data from Bessans and Aussois, the chronology of the glaciolacustrine deposits at Le Verney and Lanslebourg can be constrained. Geomorphological and stratigraphic analysis shows that these two lacustrine deposits form terraces built during the last deglaciation in the upper Maurienne Valley (Fig. 2). These two lacustrine deposits are not associated with any moraine. The morphology of the valley, showing two glacial knickpoints in this sector (Fig. 2), has favored the development of proglacial lacustrine systems rather than moraine formation, leading to the deposition of glaciolacustrine deposits. Based on deglaciation ^{10}Be cosmogenic dating conducted in the upper Maurienne valley, we infer that the formation of these glaciolacustrine systems occurred after 14.3 ka (Older Dryas) and before 12.8 ka (Younger Dryas).

3. Sedimentology, stratigraphy, and deformations

3.1. Le Verney

3.1.1. Sedimentary facies description and interpretation

The sedimentary sequence at Le Verney quarry comprises 5 sedimentary facies that can be grouped into three main facies associations (FA) based on their grain size, sedimentary structures, and geometries. Table 1 summarizes the key characteristics of each sedimentary facies and facies association. The stacking pattern of the facies associations is depicted in a panoramic photograph of the quarry (Fig. 3). Detailed sedimentary facies geometries are observable in a section 1 (Fig. 4) and log section (Fig. 5). The facies codes used in this study are derived from the classification system proposed by Miall in (1978) and (1996).

Gravels and pebbles with sandy lenses (Gcm). This facies is composed of very poorly sorted polygenic gravels and pebbles, often imbricated, with a matrix ranging in size from coarse sand to granules (see Fig. 5B–a). This deposit is characterized by sub-horizontal beds, 1–2 m thick, which can either be massive or display normal grading and sometimes terminate in levels of coarse sand. The coarse sand levels are structured with cross-lamination from climbing ripples. The facies is underlain by sub-horizontal, erosive basal boundaries (see Figs. 4 and 5).

Interpretation. The deposition of this facies is attributed to hyperconcentrated flows (Mulder and Alexander, 2001) and the presence of sandy levels indicates deposition during the energy dissipation phase of the current (Miall, 1983). The climbing ripples observed are believed to result from high sedimentation during the loss of transport capacity of a turbidity current (Ashley et al., 1982; Jopling and Walker, 1968; Mulder and Alexander, 2001).

Gravels and pebbles planar parallel stratified (Gp). This facies consists of poorly sorted polygenic gravels and pebbles showing planar parallel stratification and imbricated clasts. Bed dip is approximately 15° downstream, bed thickness ranging from 20 to 80 cm (Fig. 4). Massive beds with matrix are present, displaying either inverse or normal grading (Fig. 5B–c). These beds contain large floating clasts (50–100 cm in length) which are aligned parallel to the stratification (Fig. 4). Beds with normal or inverse grading frequently terminate in sandy levels a few tens of centimeters thick. Locally, the sedimentary structures display gravel to granule-sized scour and fill features, with sandy matrix and some clast-supported beds (Fig. 5B–b).

Interpretation. The presence of oblique planar parallel stratification and beds with normal to inverse grading suggests that sediment transport was gravity-controlled on the slope of a delta (Postma and Cruickshank, 1988; Nemec, 1990). Massive or matrix-supported beds with floating clasts are indicative of debris flow deposition (Shanmugam, 2000), while sandy levels suggest deposition during energy dissipation of concentrated or turbidity currents (Mulder and Alexander, 2001). The filling of trough structures by cross-stratification is consistent with deposition by 2D dune migration (Allen, 1982). The presence of clast supported beds with matrix-supported levels suggests that sand and gravel were separated by hydraulic processes (Carling, 1990), likely associated with a high-energy turbulent current (Allen, 1982; Carling and Glaister, 1987).

Massive gravels and pebbles (Gmg). This facies forms lenses 10–100 cm thick and approximately 10 m wide of massive poorly sorted polygenic gravels and pebbles with a matrix composed of fine sand. The grading is normal and weakly marked (Fig. 5B–d).

Interpretation. Massive, poorly sorted gravels and pebbles with sandy matrix are the result of a deposition by frictional freezing mechanism resulting from grain-to-grain interaction. Such processes correspond to a deposition by hyperconcentrated flows. The insignificant suspension fall-out generates normal and weakly marked grading

Table 1
Description of sedimentary facies, and main facies associations (FA) of Le Verney quarry.

FA	Lithofacies	Description	Geometry/ Beds contacts	Bed thickness	Interpretation
FA.1	GmgMassive gravels and pebbles.	poorly sorted gravel and pebbles with a sandy matrix, displaying normal or weak grading.	Lenticular/ Erosive	0.5–1 m	Deposition from hyperconcentrated flows.
	SsSinusoidal stratified sand with backsets.	Moderately sorted sinusoidally stratified sand (λ = 1–2 m) with low angle backset filling troughs. Large striated clasts.	Lenticular/ Erosive	0.2 to 0.1 m	Stationary or upstream migrating antidune aggradation.
FA.2	GpGravels and pebbles planar parallel stratified.	Polygenic blocks, gravels, and pebbles with a sandy matrix and parallel planar stratification. Bed dip downstream at 15°. Massive or inversely/normally graded beds terminating in a sandy layer. Presence of troughs filled with cross-stratified matrix or clast supported gravel and pebbles.	Sheet-like/ Sharp	0.8 to 0.4 m	Foreset deposits from debris flows, hyperconcentrated flows, turbidity currents, and 2D dune migration.
	ScrFine to medium sand cross-laminated.	Cross-laminated fine to medium sands indicated climbing ripple of type A (λ = 8–10 cm) and B (λ = 5–8 cm). Presence of normal grading silt-clay layers capped by convolutes. Dropstones present.	Sheet-like/ Sharp	0.05 to 0.01 m	Downstream migration of current ripples under a turbidity current losing its transport capacity. Dropstone indicate a proglacial lacustrine environment.
FA.3	GcmGravels and pebbles with sandy lenses	Subhorizontal beds of polygenic gravels and pebbles with coarse sand and granules matrix. Massive or normally graded beds terminating in a sandy layer.	Sheet-like/ Erosive	2 to 1 m	Deposit from hyperconcentrated flows, followed by a phase of flow energy dissipation.

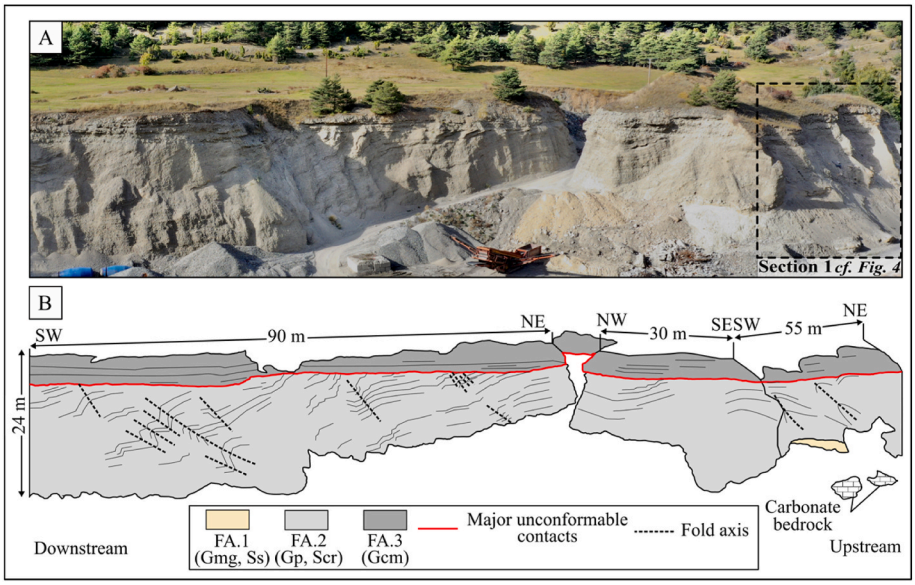

Fig. 3. (A) A panoramic photography of Le Verney quarry and localization of the interpreted section. Le Verney quarry section is described and interpreted in Fig. 4 (B) Sketch of the three facies associations (FA1, FA2 and FA3) of Le Verney quarry. The flat topography at the top of the quarry is at 1250 m asl.

(Mulder and Alexander, 2001).

Fine to medium sand cross-laminated (Scr). This facies consists of lenticular units that are 6–8 m long and 20 cm to 3 m thick, composed of well sorted fine to medium sand with cross-lamination (Fig. 4). Some basal contacts are erosive. Scr facies shows type A climbing ripples, with wavelengths of 8–10 cm and 2–3 cm in amplitude. Sinusoidal laminations corresponding to climbing ripples of type B are also present, with wavelengths between 5 and 8 cm and heights of 1–2 cm (Fig. 5B–f), as defined by Jopling and Walker (1968). Scr facies is interbedded with normally graded beds that are 5–15 cm thick, composed of fine sand or silt with parallel lamination at the base, and massive or parallel-laminated silty-clay levels with convolutions at the top (Fig. 5B–e). Isolated pebbles are visible in this facies (Fig. 5B–f). Scr sedimentary structures indicate paleocurrents variable in direction towards the southwest or southeast.

Interpretation. The cross-lamination observed in this facies is small-scale and indicative of deposition by 3D ripples under a subcritical current. The presence of climbing ripples suggests sedimentation from a current with a decreasing transport capacity. Thus, type A climbing ripples are formed when the rate of aggradation is lower than the migration rate (Jopling and Walker, 1968; Ashley et al., 1982). Conversely, type B climbing ripples are produced by a higher rate of aggradation compared to the migration rate (Jopling and Walker, 1968; Ashley et al., 1982; Allen, 1973; Fielding, 2006). These structures are the result of a low-density turbidity current (Ashley, 1995; Mulder and Alexander, 2001). The significant thickness of these ripples and climbing ripples units suggests that relatively long-duration turbidity currents are responsible for their deposition (Mulder and Alexander, 2001). Erosion surfaces are interpreted as channels that accommodated the turbidity currents. Normal grading beds are the result from of deposition during the dissipation of the energy of a low-density turbidity current (Mulder and Alexander, 2001). Isolated pebbles are dropstones that have fallen through a water column, likely resulting from iceberg melting.

Sinusoidal stratified sand with backsets (Ss): This described facies is located directly above the carbonate substratum. The granulometry consist of fine sand to granules moderately sorted. Sedimentary structures are mainly represented by sinusoidal stratification with wavelengths ranging from 1 to 2 m and an amplitude of 5–30 cm. In

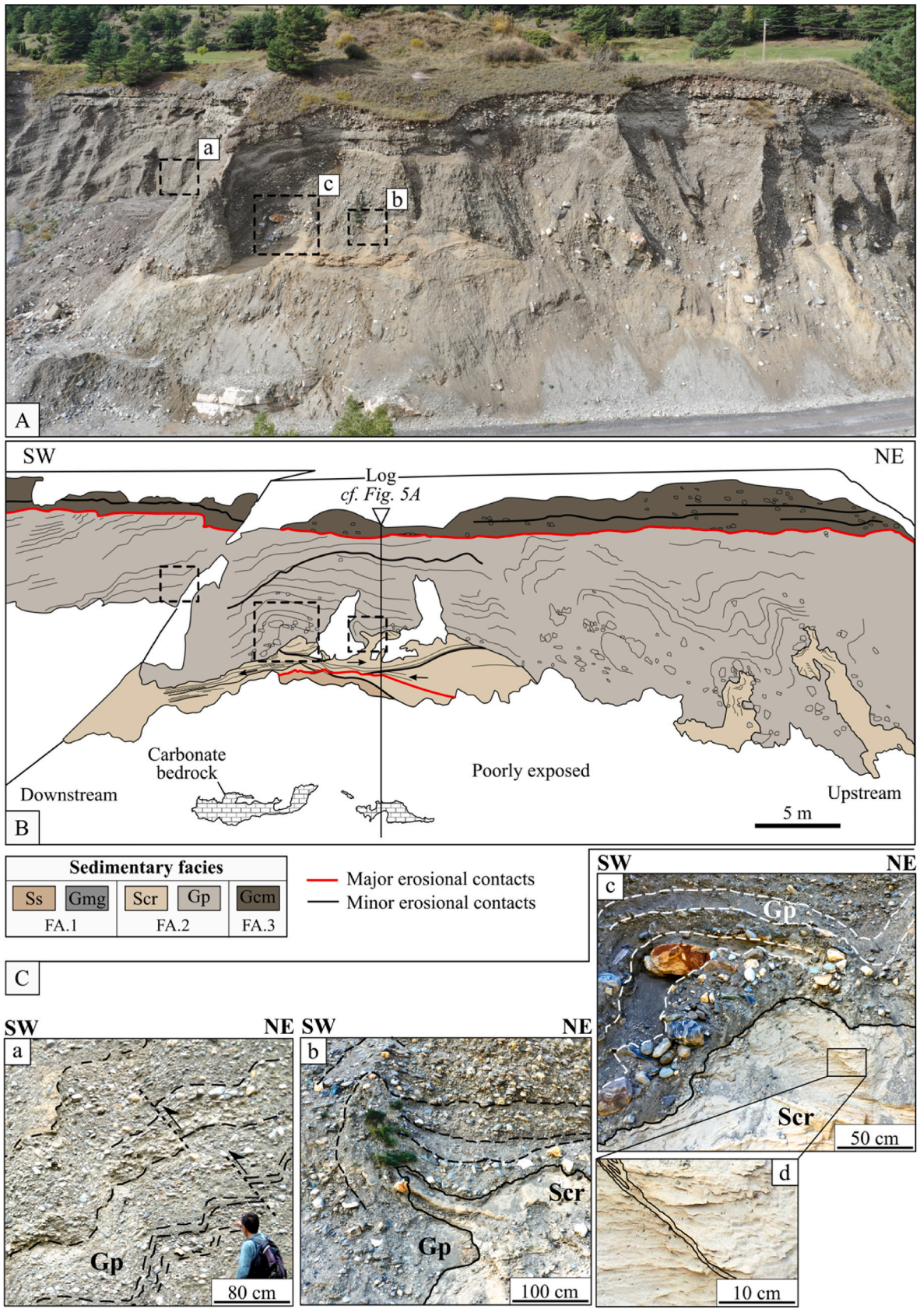

Fig. 4. Interpreted section 1 and photographs of deformation structures at the Le Verney quarry: (A) Photography of the section and localization of photographs a, b and c. (B) Sketch of the sedimentary facies associations and sedimentological log localization. (C) Photographs of the deformations. (a) Gp facies displaying reverse faults associated with antiforms and synforms. (b) Compression wedges of Scr under Gp facies. (c) Overturned southwestward vergence fold above Scr facies intrusion displaying thin per ascensum dyke. (d) Focus on the Scr facies intrusion with a better exposed fluid escape feature and per ascensum dyke.

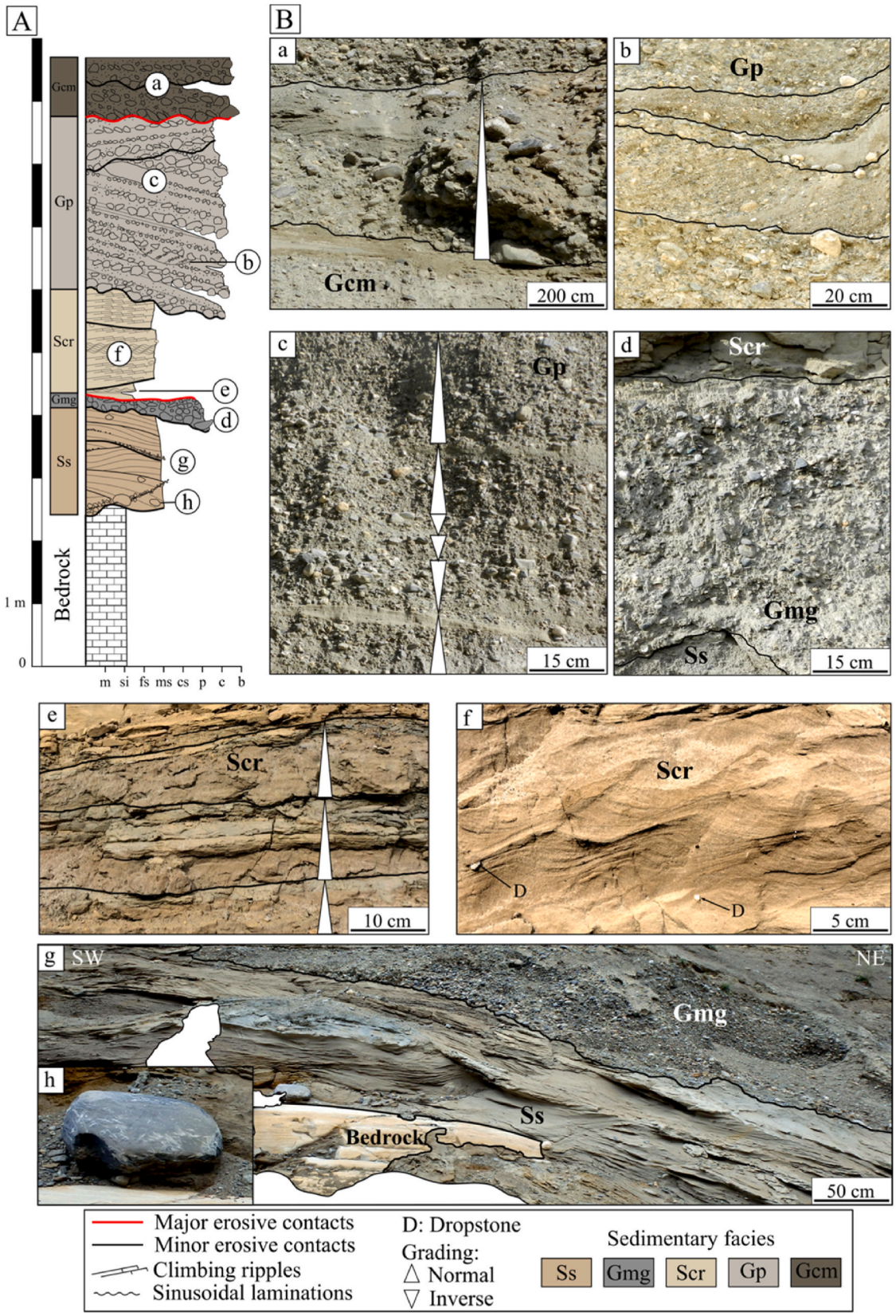

Fig. 5. (A) Sedimentary log of Le Verney quarry. (B) Photographs of the sedimentary facies of Le Verney quarry. (a) Normal grading bed of Gcm facies. (b) Trough fill by cross-stratified gravel find on Gp facies. (c) Normal and inverse graded beds and sandy layers of Gp facies. (d) Gmg facies interbedded with Ss and Scr facies. (e) Sand and silt normal graded beds of Scr facies. (f) Sand cross-laminated of facies Scr with some isolated pebbles (D). (g) Sinusoidal stratified sand with backsets of facies Ss on carbonated bedrock and overlaid by Gmg facies. (h) Striated pebble in the facies Ss. Log location is given in Fig. 4.

addition, there are also low-angle backsets beds filling troughs that are 1–2 m long, with some erosive basal contacts (Fig. 5B–g). This facies also contains striated clasts ranging from gravel to pebble (Fig. 5B–h). These clasts are aligned parallel to the stratification or occur as isolated clasts.

Interpretation: The sinusoidal stratification observed in this facies is the result of stationary antidunes aggradation under a supercritical flow, permitting the preservation of stoss and lee faces of the morphology (Cheel, 1990; Brennand, 1994; Russell and Arnott, 2003; Ito and Saito, 2006; Duller et al., 2008; Ito, 2010). Erosive contacts suggest that aggradation was not continuous (Duller et al., 2008). The low-angle backsets indicate deposition on the stoss side of counter-migrating antidunes (Kennedy, 1963; Alexander et al., 2001; Cartigny et al., 2014). The presence of coarse beds reflect deposition during high-energy conditions (Lee et al., 2015). Finally, isolated striated pebbles observed in this facies are believed to originate from the melting of debris-rich iceberg basal ice.

3.1.2. Deformations structures within facies

Description. In the Scr and Gp sedimentary facies, deformation structures include dykes, fluid escapes, fault and folds (Fig. 4). Scr is injected into the Gp facies in the northeast of the outcrop where it can form 5–10 m high intrusions (Fig. 4B). Scr is sometimes injected southwestward into Gp displaying a compressional wedge morphology approximately 1 m in length and 30 cm in thickness (Fig. 4C–b). The intrusions also contain millimetric to centimetric fluid escape features and per *ascensum* dykes (Fig. 4B–c and Fig. 4B–d).

Gp sedimentary facies displays reverse faults that are linked to antiforms and synforms with fold axes dipping at an angle of 60–70° towards the NE. These features are predominantly exposed on the NE-SW oriented sections of the quarry. The faults have a dip of at approximately 45° and are oriented towards the northeast (Fig. 3 and Fig. 4C-a). To the northeast of the outcrop, the Gp facies, located above the Scr intrusions, displays overturned folds with a south-westward vergence and located above the Scr intrusions (Fig. 4C–c).

Interpretations. The intrusion of the Scr facies into the Gp facies is related to a difference in density and viscosity between the two sediments (Hindmarsh and Rijsdik, 2000). Fluid overpressure resulting from overload by ice generates expansion and a decrease in density of the underlying sediment (Boulton and Caban, 1995). In the case of a sandy sediment charged with water and low viscosity, this decrease in density can generate a sandy intrusion into an overlying sediment of higher density (Owen, 2003; Rijsdijk et al., 2010). Fluid escape features on Scr indicate expulsion of water contained in the porosity of a sediment. In subglacial environments, fluid escape result from pressurization of water during a glacial advance or overload due to the mass of ice (Denis et al., 2009). The per *ascensum* dykes on Scr come from a glacitectonic hydrofractures under low ice overburden pressure allowing upwards release of overpressurized meltwater (Boulton et al., 1993; Boulton and Caban, 1995). Wedges occur during simple shear, allowing a sediment to inject into another overlying deposit. These structures result from glacial advances creating shear conditions. The north-eastward dip of the wedge indicates a glacial advance downstream (Rijsdijk et al., 2010).

The antiforms and synforms associated with the reverse faults evidenced in the Gp facies indicate ductile deformation associated with compressive stress (Denis et al., 2009). Orientation of the fold axis of Gp suggests NE-SW oriented compressive stress. The overturned folds are a result of ductile deformation in a sediment containing pressurized water. These folds are located above sandy intrusions, indicating that the upward vertical movement causing the intrusions is also responsible for the development of the folds. The south-westward vergence of the overturned folds implies the application of a stress (McCarroll and Rijsdijk, 2003) from the northeast associated with the glacier's advance.

3.1.3. Facies organization and depositional environment

Facies Association 1 (FA1): Subaquatic proglacial fan deposits. The FA 1 (Table 1 and Fig. 3) forms a lens-shaped set deposit of about 5 m in apparent length. The individual contained facies are also lens-shaped. FA1 association (Fig. 5) comprises sinusoidally stratified sand with backsets (Ss) and massive gravels and pebbles (Gmg). Sinusoidal stratified sand with backsets (Ss) was observed directly overlying the carbonate substrate, forming a lens 4–5 m in length. Ss is locally covered by a lens of massive gravels and pebbles (Gmg) (Fig. 5).

Interpretation: The Ss facies is related to stationary antidunes under a supercritical flow deposit directly on the bedrock, and the presence of striated pebbles in FA1 indicates a very subaquatic proximal proglacial environment. Antidunes can occur in subaquatic proglacial lacustrine environments at the outlet of a subglacial tunnel (Tracy and Brennand, 2000). The Gmg facies is associated with hyper-concentrated flows that are likely to develop in subaquatic proglacial fan which is fed by high-energy currents exiting a subglacial tunnel (Russell and Arnott, 2003; Hornung et al., 2007).

Facies Association 2 (FA2): Glaciolacustrine deltaic deposits. The FA 2 (Table 1 and Fig. 3) consists of a unit extending approximately 200 m in length and maximum thickness of about 25 m. FA2 association (Fig. 5) display at the base, fine to medium sand cross-laminated (Scr) forms lenses of 5–10 m in length, resting on the subaquatic proglacial fan deposits (FA1). The fine to medium sand cross-laminated (Scr) is overlain by gravels and pebbles planar parallel stratified (Gp). Gravels and pebbles planar parallel stratified (Gp) are observed to locally rest on sandy lenses (FA2) along an erosive contact (Fig. 5), though at the base of these lenses is occasionally not visible.

Interpretation. The Scr facies indicates a transition to a lacustrine environment, as suggested by the presence of dropstones within the facies (Fig. 5B–f). It also indicates the presence of turbidity events, which can result in the formation of small lobes, leading to the observed variability of the observed paleocurrents (Wisemann et al., 2009). Sandy turbidites deposits are common in prodeltaic facies. They are generated by relatively stable hyperpycnal currents over time, fed by river inputs (Mulder and Alexander, 2001; Wisemann et al., 2009; Gruszka and Zielinski, 2021). The inclination of the parallel planar stratification of Gp indicates a foreset facies in a deltaic environment. Specifically, the steep slope of the foresets at 15° is typical of Gilbert deltas (Gruszka and Zielinski, 2021). For this type of delta, the deposition is gravitational, and sediment transport is the result of debris flows or turbidity currents (Gruszka and Zielinski, 2021), recorded by the Gp facies. Fillings of trough structures correspond to localized channel fillings on a delta slope (Bornhold and Prior, 2009; Nemec, 1990).

Facies Association 3 (FA3): Fluvial or fluvioglacial deposit. The FA 3 (Table 1 and Fig. 3) forms a sub-horizontal layer of approximately 200 m long and 3–4 m in thickness. FA3 association (Fig. 5) is composed of gravels and pebbles with sandy lenses (Gcm) that follow an erosive contact with the FA 2. The top of this facies association corresponds to a flat and subhorizontal surface (Fig. 3).

Interpretation. The Gcm facies is composed of polygenic elements (Hugonin, 1988) and indicates a fluvial or fluvioglacial deposit mainly resulting from high-energy currents that formed sub-horizontal layers (Ethridge and Wescott, 1984; Rohais et al., 2008). FA 3 represents a fluvial or fluvioglacial event that occurred after the deposition of FA 2. Furthermore, the absence of deformations in FA3 suggests that it is also posterior to the glacier advance.

3.2. Lanslebourg

3.2.1. Sedimentary facies description and interpretation

The sedimentological and stratigraphic succession in the main outcrop of Lanslebourg is composed of 7 sedimentary facies, each defined on its grain size, sedimentary structures, and geometries. The outcrop is a subvertical unstable 45 m high cliff (Fig. 6). These sedimentary facies have been grouped into two facies associations (FA) representing depositional environments. The main characteristics of each sedimentary facies and the facies composition of the facies associations are summarized in Table 2, illustrated in a panoramic

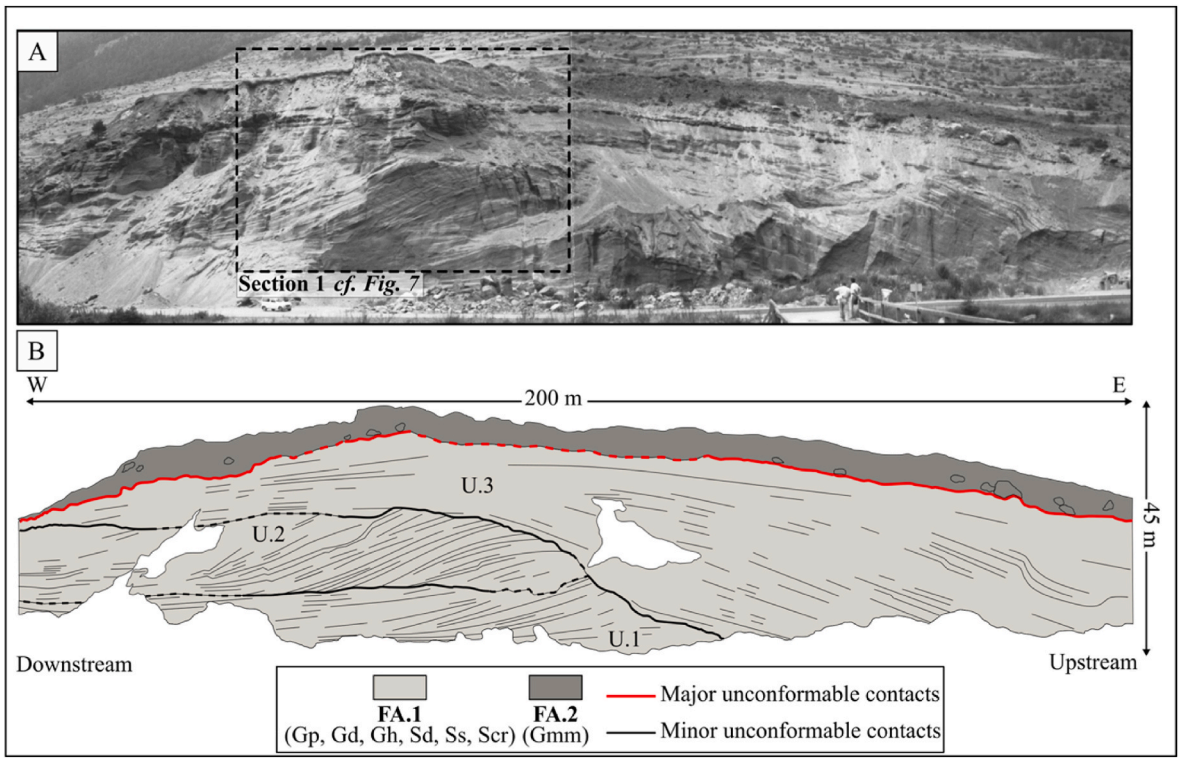

Fig. 6. (A) An old panoramic photograph of the Lanslebourg quarry from Hugonin (1988), and localization of the interpreted section. Lanslebourg quarry Section is described and interpreted in Fig. 7 (B) Organization of the two facies associations of the Lanslebourg quarry. U.1: Unit 1; U.2: Unit 2; U.3: Unit 3. The top of the FA.2 is located at an altitude of 1415 m.

Table 2
Classification of sedimentary facies and facies associations (FA) of Lanslebourg quarry.

FA	Lithofacies	Description	Geometry/ Beds contacts	Bed thickness	Interpretation
FA.1	GpPlanar and trough cross-stratified gravel and pebbles.	Gravel and pebbles with matrix of coarse sand and granules. Gravel and pebbles show a trough cross-stratification with sigmoidal and tangential foreset, cross-beds dip at 15–30°.	Lenticular/ Erosive	1.2 to 0.2 m	Deposition by migration of 2D and 3D dunes under high-energy subcritical flows under a high rate of sedimentary aggradation during hydraulic jump.
	GdPoorly sorted gravel and pebble.	Gravels and pebbles with sandy and clayey matrix displaying poorly bedded to massive strata. The grading is not visible.	Sheet-like/ Sharp	3 to 1 m	Deposition after transport by hyperconcentrated flows.
	GhPlanar-stratified gravel.	Gravels with low-angle cross-stratification (approximately 3°) and gently upstream dipping plane stratification. Normal grading beds composed of a basal clast supported layer passing upwards to poorly sorted levels containing a coarse sand matrix, sometimes terminate upward by sandy layer couplet.	Sheet-like/ Sharp	2 to 1 m	Downstream migrating antidunes and undertow progradation on stoss side of large-scale morphologies formed in a supercritical flow.
	SdDiffusely graded sand.	Medium sand and gravel diffusely graded with some beds of massive sand. Troughs filled with planar to convex upwards and upstream divergent backsets cross stratification This facies contains sandy intraclasts.	Sheet-like/ Sharp	1 to 0.5 m	Migration of stable antidunes during hydraulic jump.
	SsSinusoidal stratified sand	Sand and gravelly sand showing sinusoidal stratification ($\lambda = 4–8$ m). The sinusoidal stratification transitions to a concave-up and divergent stratification upstream.	Sheet-like/ Sharp	1.5 to 0.2 m	Deposition by stationary aggrading antidunes under a stable supercritical flow.
	ScrCross-laminated sand	Medium sand cross-laminated forming by climbing ripples of type A ($\lambda = 5–6$ m) and climbing sand and clay ripples of type B ($\lambda = 4–5$ cm) with dropstones.	Sheet-like/ Sharp	0.01–0.02 m	Deposition under subcritical conditions with a high sedimentation rate. Dropstone indicates a proglacial lacustrine environment.
FA.2	GmmMatrix-supported massive gravel.	Matrix-supported diamicton with sandy to clayey matrix. Polygenic clast from gravel to boulders, frequently facetted, polished and striated.	Sheet-like/ Erosive	3–6 m	Deposition by glacigenic processes (subglacial till).

photograph of the Lanslebourg quarry (Fig. 6) and can be more precisely observed in section 1 (Fig. 7) and log section (Fig. 8). The facies codes used in this study are derived from the classification system proposed by Miall (1978), (1996) and from Russell & Arnott (2003).

Cross-laminated sand (Scr). This facies forms units of 2–4 m thick (Fig. 7B). It predominantly comprises well sorted medium sand exhibiting cross-lamination. Within the Scr facies, climbing ripples of type A, 5–6 cm long and 1–2 cm high, and climbing sand and clay ripples of type B, 4–5 cm long and 1 cm high are observed (Fig. 8B–i) as defined by Jopling and Walker (1968). Some dropstones are visible within this

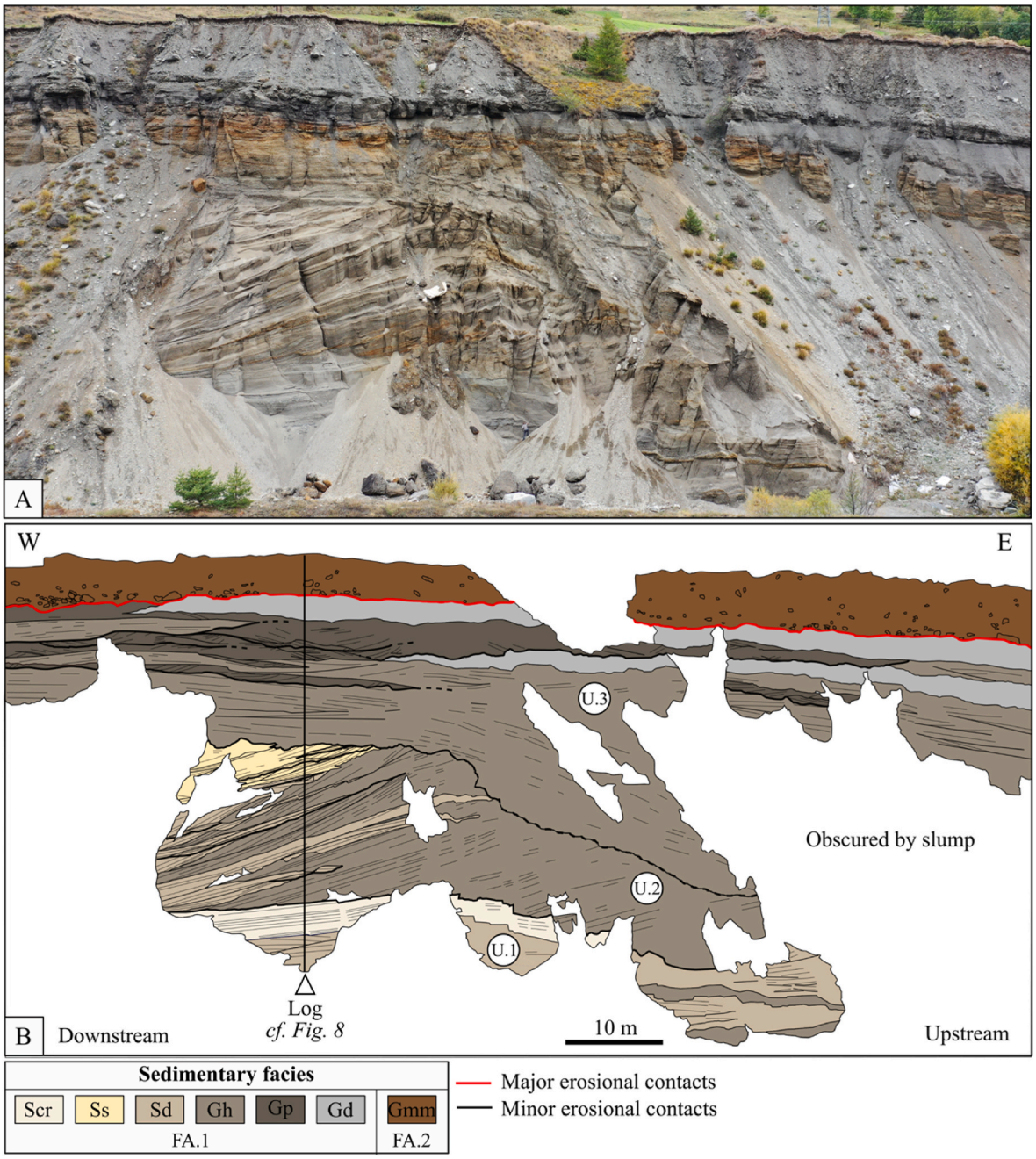

Fig. 7. Interpreted section 1 of the Lanslebourg quarry (A) Photography of section. (B) Sketch of sedimentary facies arrangement and sedimentological log localization.

facies (Fig. 8B–i).

Interpretation. Small-scale cross-lamination indicates deposition resulting from the migration of sand waves under a subcritical current. The occurrence of climbing ripples indicates a high sedimentation rate caused by a current with a decreasing transport capacity. Type A climbing ripples are formed when aggradation rate is lower than the migration rate, while type B climbing ripples are produced when the aggradation rate exceeds the migration rate (Jopling and Walker, 1968; Ashley et al., 1982). Relatively thick cross-laminated sand deposits are commonly observed in glaciolacustrine environments (Jopling and Walker, 1968; Rust and Romanelli, 1975; Gorrell and Shaw, 1991). Finally, the presence of dropstones corresponds to sediments released during iceberg melting in proglacial lake.

Planar-stratified gravels (Gh). This facies consists of beds that can extend several tens of meters in length and have a thickness ranging from 1 to 2 m (Fig. 7B). It primarily consists of poorly sorted gravels exhibiting very low-angle cross-stratification at approximately 3°. The lower contacts of beds are irregular and can form large scours. Locally, Gh shows a gently upstream dipping plane stratification passing downstream to the low-angle cross-stratification (Fig. 7B). The gravels form thin layers, few decimeter-thick, with normal grading beds composed of a basal clast supported layer of 2–6 cm thick, transitioning upwards to poorly sorted levels 6–20 cm thick and containing a coarse sand matrix (Fig. 8B–e). These beds are sometimes capped by sandy layers couplet.

Interpretation: The presence of couplets of sandy layers and clasts supported beds suggests deposition under supercritical flow conditions (Collinson and Thompson, 1989; Carling, 1990; Blair, 2000). The low-angle cross-stratification results from deposition related to antidune migration (Brennand, 1994; Blair, 2000; Russell and Arnott, 2003;

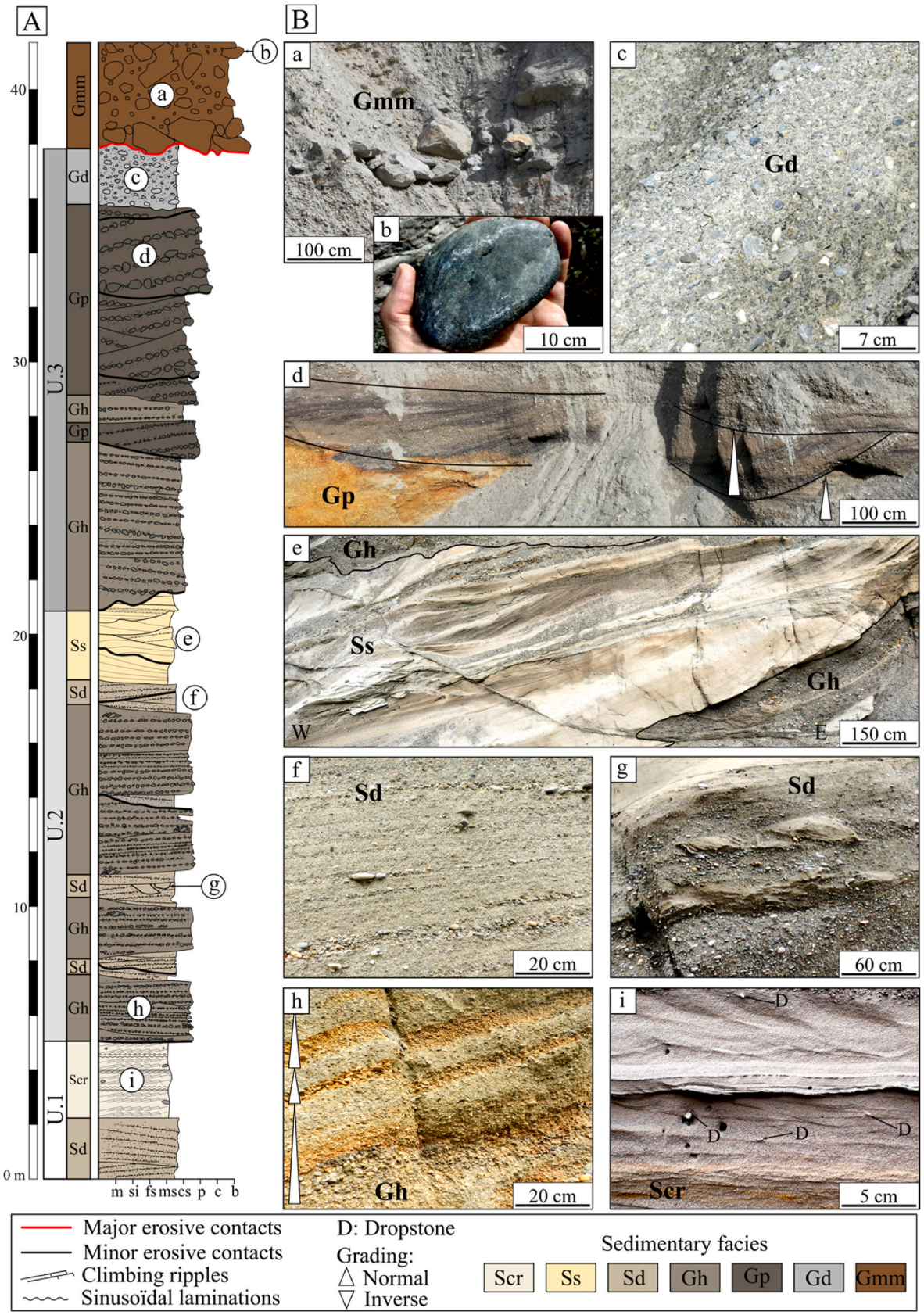

Fig. 8. (A) Sedimentary log of the Lanslebourg quarry. (B) Photography of the sedimentary facies of the Lanslebourg quarry. (a) Gmm facies with large boulders. (b) Striated pebble on Gmm facies. (c) Gd facies. (d) Through cross bedded and sigmoidal foresets of Gp facies. (e) Sinusoidal, concave-up upstream divergent stratification and massive beds of Ss facies interbedded by Gh facies. (f) Diffusely graded sand and gravel of Sd facies. (g) Example of sandy intraclasts find on Sd facies. (h) Normal grading sequences with clast and matrix supported layers of Gh facies. (i) Cross-laminated sand of Scr facies with silty laminae and dropstones. Log location is given in Fig. 7.

Duller et al., 2008; Lang and Winsemann, 2013; Froude et al., 2017). The absence of backsets indicates significant downstream migration of the antidunes (Ito, 2010; Cartigny et al., 2014; Fedele et al., 2016; Lang et al., 2017a, 2017b). The upstream dipping plane stratification observed is characteristic of underflow progradation on stoss side of large-scale morphologies formed by a supercritical flow. Further downstream, the low-angle cross-stratification results from the progradation on the lee side of the antidunes (MacDonald et al., 2009; Lang and Winsemann, 2013).

Diffusely graded sand (Sd). This facies consists of beds ranging from 10 to 30 m in apparent length and with a thickness of 0.5–1 m, displaying sub-horizontal stratification. The basal boundaries of the sequences can either be flat or form irregular troughs, which are subsequently filled with backsets. These backsets are planar to convex upwards and diverge in an upstream direction (Fig. 7). Sd is predominantly composed of poorly sorted medium sand and gravels diffusely graded, with occasional beds of well-sorted massive sand (Fig. 8B–f). Additionally, this facies contains sandy intraclasts measuring 20–30 cm in length (Fig. 8B–g).

Interpretation. The diffuse grading observed in the sandy fill and the presence of beds of massive sand suggest rapid deposition from a sediment-laden current (Russell and Arnott, 2003). The units filling the trough structures come from erosion and deposition by hydraulic jumps (Alexander et al., 2001; Fielding, 2006; Lang and Winsemann, 2013; Cartigny et al., 2014). The upward convex geometry of backsets, along with the sub-horizontal stratification, indicate deposition occurring during the migration of stable antidunes (Alexander et al., 2001; Fielding, 2006; Duller et al., 2008; Lang and Winsemann, 2013; Cartigny et al., 2014). The presence of sandy intraclasts can be attributed to erosion followed by rapid deposition of sandy beds associated with a hydraulic jump (Gorrell and Shaw, 1991; Brennand, 1994; Russell and Knudsen, 1999).

Sinusoidal stratified sand (Ss). This facies forms a unit with an apparent length of 20 m and a maximum visible thickness of 7 m. The lower contacts exhibit either planar or erosive morphologies (Fig. 7B). Ss facies primarily comprises well-sorted sand that transitions towards moderately sorted gravelly sand, displaying sinusoidal stratification. The wavelength of the sinusoidal stratification ranges between 4 and 8 m. As the stratification progresses upstream, it transitions to a concave-up and divergent stratification. The amplitude of the sinusoidal stratification decreases downstream and transforms into sub-horizontal stratification (Fig. 8B–e).

Interpretation. The presence of sinusoidal stratification in this facies suggest a deposition by stationary aggrading antidunes under a relatively stable supercritical flow. Moreover, such stratification appears during high sedimentation rates (Jopling and Walker, 1968; Allen, 1973; Fielding, 2006). Such conditions allow for the preservation of the stoss and lee sides of the antidunes (Cheel, 1990; Brennand, 1994; Russell and Arnott, 2003; Ito and Saito, 2006; Duller et al., 2008; Ito, 2010). The erosive boundaries indicate episodes of non-continuous aggradation (Duller et al., 2008). Furthermore, the concave-up and divergent stratification can be interpreted as deposition due to aggrading antidunes (Lang and Winsemann, 2013).

Planar and trough cross-stratified gravels and pebbles (Gp). This facies forms extensive sheets layers 100 m long and ranging from 5 to 8 m in thickness (Fig. 7B). Gp facies consist of poorly sorted gravels and pebbles in a matrix of coarse sand and granules. Gravels and pebbles show a trough cross-stratification with sigmoidal and tangential foresets, cross-beds dip at 15–30°. Normally graded cross-beds are sometimes visible (Fig. 8B–d). Irregular scours ranging from 20 to 30 m long and 1 m thick are visible on the sketch (Fig. 7B).

Interpretation. Planar and trough cross-stratification are formed when sedimentary layers are deposited by migration of two and three-dimensional subaqueous dunes respectively (Allen, 1984; Allen and Homewood, 1984). Specifically, sigmoidal and tangential foreset indicate a high rate of sedimentary aggradation during the transition from dunes to upper-stage plane beds, under high-energy subcritical flows (Fielding, 2006). The presence of normally graded cross-beds suggests gravity sorting by slipface avalanching (Russell and Arnott, 2003). The numerous scours observed in the deposit indicate a scour and fill deposit. The high rate of sedimentation rate, occurrence of scour fill and presence of high-energy subcritical flows are consistent with a deposition induced by hydraulic jump.

Poorly sorted gravels and pebbles (Gd). This facies comprises beds that extend up to one hundred meters in length and have a thickness ranging from 1 to 3 m. The lower boundaries of the beds are well-defined and are sharp (Fig. 7B). Gd display weakly bedded strata or massive strata composed of poorly sorted gravel and pebbles with a sandy and clay matrix. It is composed of poorly bedded to massive strata of poorly sorted gravels and pebbles with sandy and clayey matrix (Fig. 8B–c).

Interpretation. The presence of poorly sorted gravels and pebbles with clayey and sandy matrix result from deposition after transport by hyperconcentrated flows. These sedimentary characteristics indicate turbulent transport and limited sorting of sediment particles. (Mulder and Alexander, 2001).

Matrix-supported, massive gravels (Gmm). Gmm consist of matrix-supported diamicton with sandy to clayey matrix. Clasts are polygenic and their size vary from gravels to boulders, with the largest observed boulder reaching 2 m long. Clasts are frequently facetted, polished and striated (Fig. 8B–b). The base of the diamicton is constituted by a boulder's pavement over 20 m in extent (Fig. 8B–a).

Interpretation. Multimodal clast-size distribution and the facetted and striated clasts indicate the formation of diamicton at the glacier bed. The boulder pavement is associated with a till base or may result from a subglacial erosion (Lesemann et al., 2010).

3.2.2. *Facies organization and depositional environment*

Facies association 1 (FA1): Subaquatic proglacial fan. This FA (Table 2 and Fig. 6) forms a sedimentary sequence of approximately 200 m long and 35 m in height. FA1 is characterized by the presence of three units separated by unconformable and erosive contacts (Figs. 6 and 7).

Unit 1 is the more basal and measures 130 m long and has a thickness between 3 and 10 m (Fig. 6). Large-scale sedimentary structures consist of low angle tangential foreset bedding showing a dip toward the west. The dip reaches a maximum of 22° westward and becomes progressively subhorizontal westward. Unit 1 is characterized by a decrease in mean grain size toward the west (i.e., downstream), transitioning from a poorly sorted sandy gravel to well-sorted sand. Unit 1 (Fig. 8) is composed of planar-stratified gravels (Gh), diffusely graded sand (Sd) and cross-laminated sand (Scr). The lateral arrangement of these sedimentary facies suggests a supercritical condition characterized by antidune migration and hydraulic jump (Gh and Sd respectively) transitioning to a subcritical condition with cross-ripple migration (Scr) westward.

Unit 2 is 105 m long, with a thickness of 13 m (Fig. 6). Large-scale sedimentary structures in this deposit exhibit a sigmoidal to tangential foreset bedding at a dipping toward the west with a maximum angle of 24°. The foreset bedding downlaps unit 1 and becomes subhorizontal westward. This deposit consists of coarser sediment than unit 1 and displays an unconformable and erosive contact with the underlying unit. A decrease in mean grain size is observed toward the west, passing from gravel to sandy gravel. Unit 2 (Fig. 8) comprises planar-stratified gravels (Gh), diffusely graded sand (Sd) and sinusoidal stratified sand (Ss). The lateral arrangement of these facies indicates supercritical condition characterized by antidune migration (Gh) developing into to a hydraulic jump westward (Sd and Ss).

Unit 3 forms a sedimentary wedge that exhibits a decrease thickness toward the west. The sedimentary wedge extends over a length of 200 m, with a thickness ranging from 3 to 30 m (Fig. 6). The large-scale sedimentary structures within the upper unit display a concave-down eastward-dipping bedding, reaching a maximum angle of 18°, which gradually becomes sub-horizontal westward (i.e. downstream). The

bedding onlaps unit 2 and the contact between them is uncomformable and erosive. Unit 3 (Fig. 8) is characterized by coarse sediment composed of gravel and pebbles. Within this unit, we observe planar-stratified gravels (Gh), poorly sorted gravels and pebbles (Gd), as well as planar and trough cross-stratified gravels and pebbles (Gp). The lateral arrangement of these facies indicates a supercritical condition with antidune migration and hyperconcentrated flow (Gh and Gd, respectively), while a hydraulic jump is inferred in the downstream direction (Gp).

Interpretation. The occurrence of dropstones in facies Sc implies a glaciolacustrine environment. Deposits under a supercritical regime were recorded by facies Gh, Sd, and Ss. These facies are associated with deposits formed under a supercritical regime, which is a characteristic feature of ice contact deltas (Brennand, 1994; Russell and Arnott, 2003; Hornung et al., 2007; Russell et al., 2007; Leszczynska et al., 2017, 2018; Lang et al., 2017b). This environment represents the glacial margin where sediment inputs originate from glacial or subglacial conduits that discharge into a proglacial lacustrine environment (Rust and Romanelli, 1975; Powell, 1990; Gorrell and Shaw, 1991; Lonne, 1995; Le Heron et al., 2004; Hornung et al., 2007; Wisemann et al., 2009; Deschamps et al., 2013; Aquino et al., 2016). When these meltwater flows encounter stagnant water, they behave like jets, resulting in a sudden dissipation of energy through turbulence (Bates, 1953; Launder and Rodi, 1983; Hoyal et al., 2003). From proximal to distal zones relative to the glacial margin, a transition is observed between a zone of flow establishment (ZFE) and a zone of established flow (ZEF), separated by a transition zone (ZT) (Powell, 1990; Gorrell and Shaw, 1991; Russell and Arnott, 2003) (Fig. 9).

The ZFE, located in the most proximal region, display supercritical conditions (Gorrell and Shaw, 1991; Russell and Arnott, 2003). Within this zone (Fig. 9), the presence of hyperconcentrated flow (Gd) leads to the deposition of poorly sorted gravel transitioning downstream to a more diluted flow (Gh) characterized by the migration of gravel antidunes (Russell and Arnott, 2003; Hornung et al., 2007).

Downstream, the ZT shows a hydraulic jump resulting from the rapid deceleration of the current (Rajaratnam and Subramanyam, 1986; Russell and Arnott, 2003). The deposits are characterized by a high rate of aggradation, marked by facies with diffusely graded under a supercritical regime (Gorrell and Shaw, 1991; Russell and Arnott, 2003). Facies Sd and Ss provide evidence of these conditions. Episodically, erosive contact in this zone, as recorded within facies Gp, Sd and Ss indicate intermittent erosion caused by the migration of hydraulic jumps. Under the ZT zone, facies Gp (Fig. 9) record a pulse of waning flow that results in reworking of antidunes deposits by a subcritical flow, leading to the deposition of dunes (Lang and Winsemann, 2013).

In the most distal part, the ZFE is characterized by the occurrence of facies Scr (Fig. 9) which indicates low-energy conditions that allow deposition of current ripples (Russell et al., 2007).

These lateral and vertical successions of deposits, derived from supercritical flow regimes, are interpreted as the result of temporal and spatial variations in supercritical flows (Lang and Winsemann, 2013). These variations are linked to the dynamic nature of the subglacial

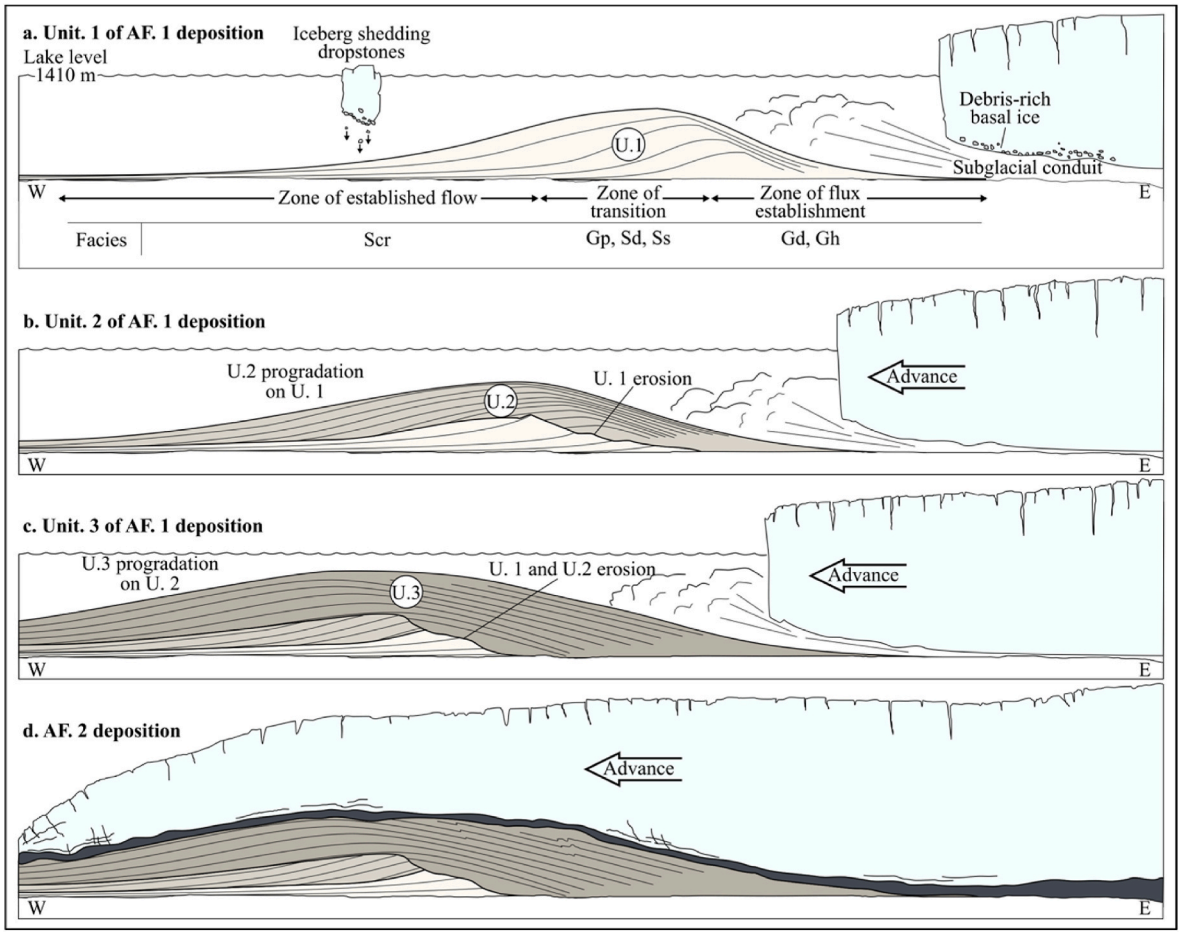

Fig. 9. Reconstruction of the depositional history of Lanslebourg basin. (a) Deposition of unit 1 with position of the zone of flux establishment (ZFE), the zone of transition (ZT) and the zone of established flow (ZEF). (b) Glacier advance and subsequent erosion of the most part of unit 1 and progradation of unit 2 on unit 1. (c) Glacier advance and subsequent erosion of most part of unit 1 and 2, progradation of unit 3 on unit 2. (d) Glacier advance on the ice contact delta deposit with deposition of a till.

proglacial fans, which exhibit high temporal and spatial instability (Russell et al., 2007). Fluctuations in sediment load also control these lateral and vertical successions (Lang and Winsemann, 2013).

From the base to the top of FA1, the facies progressively become proximal to the glacier margin. Basal unit 1 comprises facies of ZT and ZEF, while unit 2 consists of ZT and ZFE facies. Unit 3 includes ZT and ZFE facies, with a very proximal Gd facies. Within each unit, numerous interstratifications of Gp, Sd, and Ss facies are observed. These lateral and vertical successions of deposits derived from supercritical flow regimes are interpreted as resulting from temporal and spatial variations in supercritical flows regime (Lang and Winsemann, 2013), linked to the highly unstable nature in time and space of the subglacial proglacial jets (Russell et al., 2007). Fluctuations in sediment load also control these lateral and vertical successions (Lang and Winsemann, 2013).

Facies association 2 (FA2): Diamicton deposit. The FA 2 is located in the upper part of the outcrop and forms a concave down layer that is about 200 m long and 3–6 m thick (Table 2 and Fig. 6 and log Fig. 8). This deposit is composed by matrix-supported, massive gravel (Gmm) with poorly sorted sediment and forms an erosive contact with unit 3 of the FA 1.

Interpretation. Diamicton was deposited at the glacier bed as evidenced by the facetted and striated clasts. The different striation orientation indicates clast re-orientations and re-alignments during subglacial transport (Hicock, 1991; Benn, 1995).

4. Discussion

4.1. Le Verney – Proglacial lacustrine sedimentation and subsequent glacier advance

FA1 and FA2 facies associations described at Le Verney provides evidence of a significant transition in a glaciolacustrine environment, evolving from a highly proximal subaquatic proglacial fan to a proglacial Gilbert delta-type environment. This stratigraphic succession in depositional environments reflects the retreat of the Arc glacier margin on a proglacial lake.

The proglacial lacustrine facies at Le Verney show soft sediment deformations indicative of fluid overpressure, shear deformations, and compression stresses. Hydrofracturing occurs when the rapid advance of a glacier exerts significant pressure on water-saturated sediments, increasing pore water pressure and causing fractures. These sediment-filled fractures are direct evidence of such overpressure events. Per ascensum dykes, vertical intrusions of sediment through fractures, also result from significant fluid overpressure. Their vertical orientation indicates upward-directed stress consistent with glacial loading (Ravier, 2024) and reference's therein). Deformations including shear and compression structures, suggest the application of significant stress from the advancing glacier (Phillips et al., 2008), compressing and deforming the underlying sediments. Stratigraphic analysis places these deformations after the formation of Gilbert-type foresets (facies association FA2), situating the glacial re-advance after deltaic deposition. Hydrofractures and per ascensum dykes, indicating fracturing under low ice thickness in marginal positions (Ravier et al., 2015), further support the hypothesis of the Arc glacier's re-advance. These features result from fluid overpressure and the stresses exerted by the glacier, confirming the re-advance over deltaic deposits at Le Verney.

The association of facies FA3 recording fluvial or fluvioglacial processes demonstrates the final retreat phase of the Arc glacier in the Le Verney region.

4.2. Lanslebourg – Proglacial lacustrine sedimentation during glacier advance

In Lanslebourg, the facies association FA1 shows a transition of the most proximal deposition processes, characterized by an upward increase in grain size resulting from the downstream displacement of the subglacial jet (Fig. 9). These three units indicate a progressively more proximal condition during deposition, each unit undergoing partial erosion and subsequent progradation onto the previous one. This stratigraphic succession provides evidence of an advance of the glacier margin. Unit 1 represents the earliest deposited unit, which was subsequently eroded by the advance of the Arc glacier margin, while unit 2 progrades over unit 1. The erosion caused by the glacier margin affected both unit 1 and 2, with unit 3 subsequently prograding over unit 2. The upstream dip of the layers has previously been interpreted as attributed either to active tectonics or to the dissolution of gypsum at depth (Hugonin, 1988). However, based on our new sedimentological model, these hypotheses are no longer considered valid.

The facies association FA2 indicates a transition to a subglacial environment suggesting the overriding of the ice contact fans by the advancing of the Arc glacier (Fig. 9). The glacier advance is further supported by the observation of small deformations in the upstream part of the outcrop, now hidden by collapsed material. These deformations have been interpreted as resulting from compression induced by the glacier advance (Hugonin, 1988). The absence of abundant deformation in facies association FA1 implies a decoupling between basal ice and the impermeable till layer, indicative of a glacier-bed decoupling process (Ingolfsson et al., 2015).

The sedimentary facies interpretation implies the occurrence of a lake with a water level around 1410 m asl. This is approximately 15 m above the elevation of the glacial knickpoints. On the field, there is no evidence of the glacial knickpoints erosion or landslide. Therefore, this lake can only be linked to the presence of a glacial dam by the Doron glacier.

4.3. Implications of chronological data and sedimentological results for the Arc glacier dynamics

In the Maurienne Valley, the initiation of the Bølling-Allerød Interstadial is discerned by a recessionary phase of the Arc Glacier, as evidenced by ^{10}Be exposure ages obtained from erratic boulders dating at 14.27 ± 0.44 ka at Aussois (Prud'homme et al., 2020). Subsequently, the Bølling-Allerød is succeeded by an advance of the Arc Glacier, supported by ^{10}Be dating at 12.75 ± 0.36 ka at Bessans corresponding to Younger Dryas moraines (Nicoud et al., 2009).

Detailed sedimentological analyses conducted at Le Verney and Lanslebourg sites reveal distinct records of the Arc and Doron glaciers dynamic between 14.3 ± 0.4 ka and 12.8 ± 0.4 ka, aligning with the Bølling-Allerød interstadial. Notably, no preserved morainic landforms from these advances are discernible in the landscape. These observations underscore the significance of intramontane glaciolacustrine basins in precisely reconstructing the Maurienne Glacier's deglaciation history.

According to the chronological data, it is plausible to assert that lacustrine sedimentary deposits serve as proxies for stabilization stages or readvances of the Arc and Doron glaciers during the Bølling-Allerød. However, a more refined chronology would be necessary to document second order glacial oscillations in these lacustrine records. Consequently, we propose two hypotheses for the deglaciation in the upper Maurienne Valley.

A first hypothesis regarding glacial dynamics during retreat suggests that a simultaneous record was made through lacustrine sediment deposition at Le Verney and Lanslebourg sites, depicting a specific phase of readvance/stabilization of the Arc and Doron glaciers. Although Hugonin (1988) previously proposed a similar scenario, the absence of chronological data led him to attribute these stabilizations to the Oldest Dryas. However, based on the available chronological data, we find it difficult to reconcile this scenario with the previously proposed chronology. Consequently, we propose that this phase of glacier readvance/stabilization, if simultaneous, occurred during one of the cold event of the Bølling-Allerød.

A second hypothesis can be advanced, this time grounded on paleoclimatic data (Rasmussen et al., 2014; Li et al., 2021) and using our

recent sedimentological analysis of lacustrine deposits as proxies for glacier dynamics. The Older Dryas and the intra-Allerød cold events represent distinct periods characterized by favorable climatic conditions for glacier readvances. Our sedimentological analysis reveals a glacial advance at two locations during the Bølling-Allerød Interstadial. A plausible scenario therefore associates the two advances observed to the two short cold events that characterize this warming period. Following this hypothesis, according to paleoclimate proxies (Rasmussen et al., 2014; Li et al., 2021), the stabilization/readvance recorded in Le Verney basin could be correlated with the Older Dryas cold event. Conversely, the glacier readvances observed in the Lanslebourg basin could be linked to the Intra-Allerød Cold event.

4.4. Paleoclimate control on Bølling-Allerød cooling events in central Western Europe

Our new investigations in the Maurienne Valley underscore glacial advance at two locations during Bølling-Allerød interstadial. These glacial advances located respectively 21 and 12 km downstream of the moraines deposited by the subsequent advance of the Arc Glacier during the Younger Dryas (Nicoud et al., 2009), suggest a greater extension of the Arc Glacier during the cold Bølling-Allerød events. But our findings are not unique to our site. Similar observations are also reported in the western Italian Alps. Particularly in the Dora Baltea valley, a potential glacier advance or standstill marked by moraines during the Older Dryas has been suggested (Porter and Orombelli, 1982). Subsequent dating using exposure ages of ^{10}Be on glacial boulders and polished bedrock sets this event at 14.1 ka (Serra et al., 2022). Smoothed morainic ridges in Austria are chronologically correlated with the Bølling-Allerød cold pulse (van Husen, 2000). However, the temporal constraint on this glacier advance relies on indirect ^{14}C dating (Maisch, 1987), and the lack of suitable boulders prevents direct dating (Ivy-Ochs, 2015).

The two brief Bølling-Allerød interstadial cold events, GI-1d and GI-1b, described in the Greenland ice core (Rasmussen et al., 2014), have also been found in Europe using various proxies. Palynological studies or oxygen isotope analyses conducted in Switzerland (Lotter et al., 1992; Van Raden et al., 2013), alongside the annual varve count in western Germany (Brauer et al., 2000a), and in southern Germany by examining oxygen isotope fluctuations in ostracods (von Grafenstein et al., 1999). These cold events are also well documented in the nearest German stalagmites (Li et al., 2021). In addition, variations in lake levels in the Swiss Plateau, Jura and French Pre-Alps indicate an increase in precipitations in these areas during the GI-1d and GI-1b periods (Magny, 2001).

The findings of our study provide evidence supporting the occurrence of glacial advances at two locations in the Maurienne Valley probably during the Bølling-Allerød cold events. The observed glacial advances suggest a positive mass balance of the Arc glacier, indicating an increase in precipitation and drop in temperatures in the western French Alps during the Bølling-Allerød cold events.

Nevertheless, the identification of these glacial advances during the Bølling/Allerød cold events in the Alps underlines the challenge of their limited duration, which often leads to a lack of significant glacial deposits (Ivy-Ochs, 2015; Ivy-Ochs et al., 2023). In the upper Maurienne Valley, the identification of these advances has been facilitated by the exceptional preservation of glaciolacustrine deposits. However, it is probable that many other Alpine valleys lack evidence as well-preserved as the Upper Maurienne glaciolacustrine deposits. This discrepancy could be attributed to the significant glacial re-advance during the Younger Dryas, which may have eroded the geomorphological traces of earlier glacial advances associated with the short Bølling-Allerød cold events.

5. Conclusion

Detailed sedimentological, stratigraphical and soft sediment deformation analyses of the proglacial deposits at Le Verney and Lanslebourg allow the identification of short re-advances of the Arc glacier during the Bølling-Allerød climate warming in Maurienne Valley (Western Alps). At Le Verney site, a sedimentological succession highlights a retreat of the glacier margin, with deformation suggesting a subsequent glacier advance. At Lanslebourg site, the sedimentary succession reveals three ice-contact delta units, each displaying progressively more proximal conditions upward, indicating a glacier re-advance. The presence of till deposit at the top of the stratigraphic sequence further confirms a glacier advance over the ice-contact delta deposit.

Considering previous geomorphological, geochronological and sedimentological data, this paper presents evidence for one or two short glacier advances possibly associated with the Bølling-Allerød cold events, occurring within the context of global climate warming during the Bølling-Allerød. The subsequent glacier advance, as evidenced by frontal moraines at Bessans, corresponds to a period of climate cooling during the Younger Dryas.

Except for Younger Dryas moraines, the advances of the Arc glacier have not resulted in the formation of significant glacial morphologies. This study highlights the importance of proglacial lacustrine environments as archives of subtle glacial fluctuations. Sedimentological analysis of this deposits may be used as a complement to geomorphological studies, aiding in a reconstruction of past glacier fluctuations.

Given the ongoing global climate change, it is becoming important to investigate brief past glacial fluctuations to discern potential responses of mountain glaciers. Further work is needed to increase the number of regional training sets (sedimentary records, geomorphology, and cosmogenic dating analysis) during the Bølling-Allerød, thereby fostering a comprehensive understanding of glacier responses to centennial-scale climate variability. Our findings elucidate past glacial dynamics in the western Alps and supply valuable context for investigating the intricate interplay between contemporary climate warming and responses of Alpine glaciers.

CRediT authorship contribution statement

Thibault Roattino: Writing – original draft. **Jean-François Buoncristiani:** Writing – original draft. **Christian Crouzet:** Writing – original draft. **Riccardo Vassallo:** Writing – original draft.

Declaration of competing interest

The authors declare that they have no known competing financial interests or personal relationships that could have appeared to influence the work reported in this paper.

Data availability

Data will be made available on request.

Acknowledgments

The authors acknowledge financial support from the French Institut National des Sciences de l'Univers (INSU) and the Université Savoie Mont Blanc AAP DIEGO I and II. The BRGM (Bureau de Recherches Géologiques et Minières) is acknowledged for its contribution via the national program Référentiel Géologique de la France Alpes (RGF-Alpes). We are very thankful to Gerard Nicoud for sharing the raw data of the 10Be dated boulders in Bessans area, from which we could recalculate exposure ages with the updated scaling parameters. We would like to thank the two anonymous reviewers whose pertinent comments helped to improve this manuscript.

References

Alexander, J., Bridge, J.S., Cheel, R.J., Leclair, S.F., 2001. Bedforms and associated sedimentary structures formed under supercritical water flows over aggrading sand beds. Sedimentology 48, 133–152.

Allen, J.R.L., 1973. A classification of climbing-ripple cross-lamination. J. Geol. Soc. 129, 537–541.

Allen, J.R.L., 1982. Sedimentary Structures, Their Character and Physical Basis Volume 1. Elsevier, Amsterdam, p. 593.

Allen, J.R.L., 1984. Sedimentary structures: their character and physical basis. In: L Allen, J.R. (Ed.), Developments in Sedimentology. Elsevier, pp. 1–663.

Allen, P.A., Homewood, P., 1984. Evolution and mechanics of a Miocene tidal sandwave. Sedimentology 31, 63–81.

Alley, R.B., Meese, D.A., Shuman, C.A., Gow, A.J., Taylor, K.C., Grootes, P.M., White, J. W.C., Ram, M., Waddington, E.D., Mayewski, P.A., Zielinski, G.A., 1993. Abrupt increase in Greenland snow accumulation at the end of the Younger Dryas event. Nature 362, 527–529.

Aquino, C.D., Buso, V.V., Faccini, U.F., Milana, J.P., Paim, P.S.G., 2016. Facies and depositional architecture according to a jet efflux model of a late Paleozoic tidewater grounding-line system from the Itarare Group (Parana Basin), southern Brazil. J. S. Am. Earth Sci. 67, 180–200.

Ashley, G.M., 1995. Glaciolacustrine environments. In: Menzies, J. (Ed.), Modern Glacial Environments. Elsevier, pp. 417–444.

Ashley, G.M., Southard, J.B., Boothroyd, J.C., 1982. Deposition of climbing-ripple beds: a flume simulation. Sedimentology 29, 67–79.

Baroni, C., Martino, S., Salvatore, M.C., Scarascia Mugnozza, G., Schiliro, L., 2014. Thermomechanical stress-strain numerical modelling of deglaciation since the last glacial maximum in the Adamello group (Rhaetian Alps, Italy). Geomorphology 226, 278–299.

Baroni, C., Casale, S., Salvatore, M.C., Ivy-Ochs, S., Christl, M., Carturan, L., Seppi, R., Carton, A., 2017. Double response of glaciers in the upper Peio valley (Rhaetian Alps, Italy) to the younger Dryas climatic deterioration). Boreas 46, 783–798.

Bates, C., 1953. Rational theory of delta formation. AAPG (Am. Assoc. Pet. Geol.) Bull. 37, 2119–2162.

Benn, D.I., 1995. Fabric signature of subglacial till deformation. Sedimentology 42, 735–747.

Bennett, M.R., Huddart, D., Thomas, G.S., 2002. Facies architecture within a regional glaciolacustrine basin: copper River, Alaska. Quat. Sci. Rev. 21, 2237–2279.

Blair, T.C., 2000. Sedimentology and progressive tectonic unconformities of the sheetflood-dominated Hell's Gate alluvial fan, Death Valley, California. Sediment. Geol. 132, 233–262.

Bornhold, B., Prior, D., 2009. Morphology and Sedimentary Processes on the Subaqueous Noeick River Delta, British Columbia, Canada, 10. Int. Assoc. Sedimentol. Spec. Publ., pp. 169–181

Boulton, G.S., Caban, P., 1995. Groundwater flow beneath ice sheets: Part II — its impact on glacier tectonic structures and moraine formation. Quat. Sci. Rev. 14, 563–587.

Boulton, G.S., Slot, T., Blessing, K., Glasbergen, P., Leijnse, T., Vangijssel, K., 1993. Deep circulation of groundwater in overpressured subglacial aquifers and its geological consequences. Quat. Sci. Rev. 12, 739–745.

Boxleitner, M., Ivy-Ochs, S., Egli, M., Brandova, D., Christl, M., Dahms, D., Maisch, M., 2019. The ^{10}Be deglaciation chronology of the Goschenertal, central Swiss Alps, and new insights into the Goschenen Cold Phases. Boreas 48, 867–878.

Brauer, A., Endres, C., Zolitschka, B., Negendank, J., 2000a. AMS radiocarbon and varve chronology from the annually laminated sediment record of lake meerfelder maar, Germany. Radiocarbon 42, 355–368.

Brauer, A., Günter, C., Johnsen, S.J., Negendank, J.F.W., 2000b. Land-ice teleconnections of cold climatic periods during the last Glacial/Interglacial transition. Clim. Dynam. 16, 229–239.

Braumann, S.M., Schaefer, J.M., Neuhuber, S., Fiebig, M., 2022. Moraines in the Austrian Alps record repeated phases of glacier stabilization through the late glacial and the early holocene. Sci. Rep. 12, 9438.

Brennand, T.A., 1994. Macroforms, large bedforms and rhythmic sedimentary sequences in subglacial eskers, south-central Ontario: implications for esker genesis and meltwater regime. Sediment. Geol. 91, 9–55.

Briner, J.P., Kaufman, D.S., Manley, W.F., Finkel, R.C., Caffee, M.W., 2005. Cosmogenic exposure dating of late Pleistocene moraine stabilization in Alaska. Geol. Soc. Am. Bull. 117, 1108–1120.

Carling, P.A., 1990. Particle over-passing on depth-limited gravel bars. Sedimentology 37, 345–355.

Carling, P.A., Glaister, M., 1987. Rapid deposition of sand and gravel mixtures downstream of a negative step: the role of matrix infilling and particle over-passing in the process of bar-front accretion. Geol. Soc. London Spec. Publ. 144, 543–551.

Cartigny, M.J.B., Ventra, D., Postma, G., Van Den Berg, J.H., 2014. Morphodynamics and sedimentary structures of bedforms under supercritical-flow conditions: new insights from flume experiments. Sedimentology 61, 712–748.

Champagnac, J.-D., Delacou, B., Tricart, P., Sue, C., Burkhard, M., Allanic, C., 2006. Regional brittle extension in quaternary sediments of Lanslebourg (haute Maurienne valley, western Alps). Bull. Soc. Geol. Fr. 177 (4), 215–223.

Cheel, R.J., 1990. Horizontal lamination and the sequence of bed phases and stratification under upper-flow-regime conditions. Sedimentology 37, 517–529.

Chenet, M., Brunstein, D., Jomelli, V., Roussel, E., Rinterknecht, V., Mokadem, F., Biette, M., Robert, V., Léanni, L., ASTER Team, 2016. 10Be cosmic-ray exposure dating of moraines and rock avalanches in the Upper Romanche valley (French Alps): evidence of two glacial advances during the Late Glacial/Holocene transition. Quat. Sci. Rev. 148, 209–221.

Clark, P.U., Dyke, A.S., Shakun, J.D., Carlson, A.E., Clark, J., Wohlfarth, B., Mitrovica, J. X., Hostetler, S.W., McCabe, M.A., 2009. The last glacial maximum. Science 325, 710–714.

Claude, A., Ivy-Ochs, S., Kober, F., Antognini, M., Salcher, B., Kubik, P.W., 2014. The Chironico landslide (Valle Leventina, southern Swiss Alps): age and evolution. Swiss J. Geosci. 107, 273–291.

Collinson, J.D., Thompson, D.B., 1989. Sedimentary Structures. Chapmann and hall, London, p. 207.

Cossart, E., Fort, M., Bourlès, D., Braucher, R., Perrier, R., Siame, L., 2012. Deglaciation pattern during the lateglacial/Holocene transition in the southern French Alps. Chronological data and geographical reconstruction from the Clarée Valley (upper Durance catchment, southeastern France). Palaeogeogr. Palaeoclimatol. Palaeoecol. 315–316, 109–123.

Crouzet, C., Nicoud, G., Fudral, S., Rampnoux, J.P., Dzikowski, M., Paillet, A., Lacombe, P., 1999. Contrôle du remplissage détritique tardiglaciaire à holocène d'une haute vallée alpine par les dynamiques de versant : l'exemple de la moyenne Maurienne (Savoie). Quaternaire 10, 37–48.

Darnault, R., Rolland, Y., Braucher, R., Bourlès, D., Revel, M., Sanchez, G., Bouissou, S., 2011. Timing of the last deglaciation revealed by receding glaciers at the Alpine-scale: impact on mountain geomorphology. Quat. Sci. Rev. 31, 127–142.

Davis, P., Menounos, B., Osborn, G., 2009. Holocene and latest Pleistocene alpine glacier fluctuations: a global perspective. Quat. Sci. Rev. 28, 2021–2033.

Debelmas, J., 1989. Carte géologique de la France au 1/50 000, feuille 775 : Modane, notice explicative, *BRGM*, p. 144.

Denis, M., Buoncristiani, J.-F., Guiraud, M., 2009. Fluid-pressure controlled soft-bed deformation sequence beneath the surging Breiðamerkurjökull (Iceland, Little Ice Age). Sediment. Geol. 221, 71–86.

Denton, G.H., Anderson, R.F., Toggweiler, J.R., Edwards, R.L., Schaefer, J.M., Putman, A. E., 2010. The last glacial termination. Science 328, 1652–1656.

Deschamps, R., Eschard, R., Roussé, S., 2013. Architecture of late ordovician glacial valleys in the Tassili N'Ajjer area (Algeria). Sediment. Geol. 289, 124–147.

Duller, R.A., Mountney, N.P., Russell, A.J., Cassidy, N.C., 2008. Architectural analysis of a volcaniclastic jökulhlaup deposit, southern Iceland: sedimentary evidence for supercritical flow. Sedimentology 55, 939–964.

Engel, Z., Mentlík, P., Braucher, R., Křížek, M., Pluháčková, M., Arnold, M., Keddadouche, K., 2017. 10Be exposure age chronology of the last glaciation of the Roháčská Valley in the Western Tatra Mountains, central Europe. Geomorphology 293, 130–142.

Ethridge, F., Wescott, W., 1984. Tectonic setting, recognition and hydrocarbon reservoir potential of fan delta deposits. Bull. Can. Soc. Petrol. Geol. 10, 217–235.

Fedele, J.J., Hoyal, D.C., Barnaal, Z., Tulenko, J., Awalt, S., 2016. Bedforms created by gravity flows. In: Budd, D., Hajek, E., Purkis, S. (Eds.), Autogenic Dynamics in Sedimentary Systems. SEPM Spec. Publ, pp. 95–121.

Federici, P.R., Granger, D.E., Pappalardo, M., Ribolini, A., Spagnolo, M., Cyr, A.J., 2008. Exposure age dating and equilibrium line altitude reconstruction of an Egesen moraine in the Maritime Alps, Italy. Boreas 37, 245–253.

Federici, P.R., Ribolini, A., Spagnolo, M., 2017. Glacial history of the maritime Alps from the last glacial maximum to the little ice age. Geol. Soc. London Spec. Publ. 433, 137–159.

Fernandes, M., Oliva, M., Vieira, G., Palacios, D., Fernández-Fernández, J.M., Garcia-oteyza, J., Schimmelpfennig, I., Team, A., Antoniades, D., 2022. Glacial oscillations during the Bølling–Allerød interstadial–younger Dryas transition in the Ruda Valley, central Pyrenees. J. Quat. Sci. 37, 42–58.

Fielding, C.R., 2006. Upper flow regime sheets, lenses and scour fills: extending the range of architecture elements for fluvial sediment bodies. Sediment. Geol. 190, 227–240.

Froude, M.J., Alexander, J., Barclay, J., Cole, P., 2017. Interpreting flash flood palaeoflow parameters from antidunes and gravel lenses: an example from Montserrat, West Indies. Sedimentology 64, 1817–1845.

Fudral, S., 1998. Etude géologique de la suture téthysienne dans les Alpes franco-italiennes nord-occidentales de la Doire Ripaire (Italie) à la région de Bourg Saint Maurice (France). Géologie Alpine, Mémoire H.S. 29, 306p.

Fudral, S., Deville, E., Nicoud, D., Pognante, U., Guillot, P.L., Jaillard, E., Mestre, J.E., Toury-Lerouge, A., 1994. Carte géologique de la France au 1/50 000, feuille 776, 90. Lanslebourg-Mont D'Ambin, notice explicative, BRGM.

Gibbons, A.B., Megeath, J.D., Pierce, K.L., 1984. Probability of moraine survival in a succession of glacial advances. Geology 12 (6), 327–330.

Gorrell, G., Shaw, J., 1991. Deposition in an esker, bead and fan complex, Lanark, Ontario, Canada. Sediment. Geol. 72, 285–314.

Gruszka, B., Zielinski, T., 2021. Lacustrine deltas and subaqueous fans: almost the same, but different – a review. Geologos 27, 43–55.

Hartz, N., Milthers, V., 1901. Det senglaciale ler i Alleröd Teglvaerksgrav. Meddelelser Danmarks Geologisk Forening 8, 31–59.

Heyman, J., Stroeven, A.P., Harbor, J.M., Caffee, M.W., 2011. Too young or too old: evaluating cosmogenic exposure dating based on an analysis of compiled boulder exposure ages. Earth Planet Sci. Lett. 302, 71–80.

Heyman, J., Applegate, P.J., Blomdin, R., Gribenski, N., Harbor, J.M., Stroeven, A.P., 2016. Boulder height—exposure age relationships from a global glacial 10Be compilation. Quat. Geochronol. 34, 1–11.

Hicock, S.R., 1991. On subglacial stone pavements in till. J. Geol. 99, 607–619.

Hindmarsh, R., Rijsdik, K., 2000. Use of a viscous model of till rheology to describe gravitational loading instabilities in glacial sediments. Geol. Soc. London Spec. Publ. 176, 191–201.

Hoek, Z.W., 2009. Bølling-allerød interstadial. In: Gornitz, V. (Ed.), Encyclopedia of Paleoclimatology and Ancient Environments. Springer, pp. 100–103.

Hornung, J.J., Asprion, U., Winsemann, J., 2007. Jet-efflux deposits of a subaqueous ice-contact fan, glacial Lake Rinteln, northwestern Germany. Sediment. Geol. 193, 167–192.
Hoyal, D.C.J.D., Van Wagoner, J.C., Adair, N.L., Deffenbaugh, M., Li, D., Sun, T., Huh, C., Griffin, D.E., 2003. Sedimentation from Jets: A Depositional Model for Clastic Deposits of All Scales and Environments. Search and Discovery, Tulsa, OK, 74119, USA, 40082. Online-Journal., AAPG/Datapages, Inc. 1444 South Boulder.
Hugonin, F., 1988. Le Quaternaire de la haute vallée de l'Arc. Joseph Fourier University, Grenoble, France, p. 268. *Ph.D. thesis*.
Ingolfsson, O., Benediktsson, I.O., Schomacker, A., Kjaer, K.H., 2015. Glacial geological studies of surge-type glaciers in Iceland — research status and future challenges. Earth Sci. Rev. 152, 37–69.
Ito, M., 2010. Are coarse-grained sediment waves formed as downstream-migrating antidunes? Insight from an early Pleistocene submarine canyon on the Boso Peninsula, Japan. Sediment. Geol. 226, 1–8.
Ito, M., Saito, T., 2006. Gravel waves in an ancient canyon: analogous features and formative processes of coarse-grained bedforms in a submarine-fan system, the lower Pleistocene of the boso peninsula, Japan. J. Sediment. Res. 76, 1274–1283.
Iversen, J., 1942. En pollenanalytisk tidsfaestelse FA Ferskvandslagene ved Norre Lingby. Meddelelser Danmarks Geologisk Forening 10, 130–151.
Iversen, J., 1954. The Late-Glacial flora of Denmark and its relation to climate and soil. Danmarks Geologiske Undersøgelser 80, 87–119.
Ivy-Ochs, S., 2015. Glacier variations in the European Alps at the end of the last glaciation. Cuadernos de Investigacion Geografica 41, 295–315.
Ivy-Ochs, S., Kerschner, H., Kubik, P.W., Schlüchter, C., 2006. Glacier response in the European Alps to heinrich event 1 cooling: the gschnitz stadial. J. Quat. Sci. 21, 115–130.
Ivy-Ochs, S., Kerschner, H., Reuther, A., Preusser, F., Heine, K., Maisch, M., Kubik, P.W., Schlüchter, C., 2008. Chronology of the last glacial cycle in the European Alps. J. Quat. Sci. 23, 559–573.
Ivy-Ochs, S., Kerschner, H., Maisch, M., Christl, M., Kubik, P.W., Schlüchter, C., 2009. Latest Pleistocene and holocene glacier variations in the European Alps. Quat. Sci. Rev. 28, 2137–2149.
Ivy-Ochs, S., Monegato, G., Reitner, J.M., 2023. Chapter 37 - the Alps: glacial landforms from the Bølling-Allerød interstadial. In: Palacios, D., Hughes, P.D., Garcia-Ruiz, J. M., Andrés, N. (Eds.), European Glacial Landscapes - the Last Deglaciation. Elsevier, pp. 358–360.
Jaillet, S., Ballandras, S., 1999. La transition Tardiglaciaire/Holocène à travers les fluctuations du glacier du Tour (Vallée de Chamonix, Alpes du Nord françaises). Quaternaire 10, 15–23.
Jopling, A.V., Walker, R.G., 1968. Morphology and origin of ripple-drift cross-lamination, with examples from the Pleistocene of Massachusetts. J. Sediment. Petrol. 38, 971–984.
Kennedy, J., 1963. The mechanics of dunes and antidunes in erodible-bed channels. J. Fluid Mech. 16, 521–544.
Kerschner, H., 1980. Outlines of the climate during the egesen advance (younger Dryas, 11 000 - 10 000 BP) in the central Aps of the western Tyrol, Austria. Zeitschrift fur Gletscherkd und Glazialgeol 16, 229–240.
Kerschner, H., Ivy-Ochs, S., 2008. Palaeoclimate from glaciers: examples from the eastern Alps during the alpine lateglacial and early Holocene. Global Planet. Change 60, 58–71.
Kilian, W., Révil, J., 1917. Sur l'histoire de la vallée de l'Arc (Maurienne) à l'époque pléistocène. C. R. Acad. Sci. Paris 138–141.
Lang, J., Winsemann, J., 2013. Lateral and vertical facies relationships of bedforms deposited by aggrading supercritical flows: from cyclic steps to humpback dunes. Sediment. Geol. 296, 36–54.
Lang, J., Brandes, C., Winsemann, J., 2017a. Erosion and deposition by supercritical density flows during channel avulsion and backfilling: field examples from coarse grained deepwater channel-levee complexes (Sandino Forearc Basin, southern Central America). Sediment. Geol. 349, 79–102.
Lang, J., Sievers, J., Loewer, M., Igel, J., Winsemann, J., 2017b. 3D architecture of cyclic-step and antidune deposits in glacigenic subaqueous fan and delta settings: integrating outcrop and ground-penetrating radar data. Sediment. Geol. 362, 83–100.
Lang, J., Le Heron, D.P., Van den Berg, J.H., Winsemann, J., 2021. Bedforms and sedimentary structures related to supercritical flows in glacigenic settings. Sedimentology 68, 1539–1579.
Launder, B., Rodi, W., 1983. The turbulent wall jet measurements and modeling. Annu. Rev. Fluid Mech. 15, 429–459.
Le Heron, D.P., Sutcliffe, O., Bourgig, K., Craig, J., Visentin, C., Whittington, R., 2004. Sedimentary architecture of Upper Ordovician tunnel valleys, Gargaf Arch, Libya: implications for the genesis of a hydrocarbon reservoir. GeoArabia 9, 137–160.
Lee, J.R., Wakefield, O.J., Phillips, E., Hughes, L., 2015. Sedimentary and structural evolution of a relict subglacial to subaerial drainage system and its hydrogeological implications: an example from Anglesey, north Wales, UK. Quat. Sci. Rev. 109, 88–105.
Lesemann, J.-E., Aslop, G.I., Piotrowski, J.A., 2010. Incremental subglacial meltwater sediment deposition and deformation associated with repeated ice-bed decoupling: a case study from the Island of Funen, Denmark. Quat. Sci. Rev. 29, 3212–3229.
Leszczynska, K., Boreham, S., Gibbard, P., 2017. Middle Pleistocene ice-marginal sedimentation in the transitional zone between the constrained and unconstrained ice-sheet margin, East Anglia, England. Boreas 46, 697–724.
Leszczynska, K., Boreham, S., Gibbard, P., 2018. Middle Pleistocene ice-marginal sedimentation at a constrained ice-sheet margin, East Anglia, UK. Boreas 47, 1118–1143.
Li, H., Spötl, C., Cheng, H., 2021. A high-resolution speleothem proxy record of the Late Glacial in the European Alps: extending the NALPS19 record until the beginning of the Holocene. J. Quat. Sci. 36, 29–39.
Lifton, N., Sato, T., Dunai, T.J., 2014. Scaling in situ cosmogenic nuclide pro-duction rates using analytical approximations to atmospheric cosmic-ray fluxes. Earth Planet Sci. Lett. 386, 149–160.
Lonne, I., 1995. Sedimentary facies and depositional architecture of ice-contact glaciomarine systems. Sediment. Geol. 98, 13–43.
Lonne, I., Nemec, W., Blikra, L.H., lauritsen, T., 2001. Sedimentary architecture and dynamic stratigraphy of a marine ice-contact system. J. Sediment. Res. 71, 922–943.
Lotter, A.F., Eicher, U., Siegenthaler, U., Birks, H.J.B., 1992. Lateglacial climatic oscillations as recorded in Swiss lake sediments. J. Quat. Sci. 7, 187–204.
MacDonald, R., Alexander, J., Bacon, J., Cooker, M., 2009. Flow patterns, sedimentation and deposit architecture under a hydraulic jump on a non-eroding bed: defining hydraulic-jump unit bars. Sedimentology 56, 1346–1367.
Mackintosh, A.N., Anderson, B.M., Pierrehumbert, R.T., 2017. Reconstructing climate from glaciers. Annu. Rev. Earth Planet Sci. 45 (1), 649–680.
Magny, M., 2001. Palaeohydrological changes as reflected by lake-level fluctuations in the Swiss Plateau, the Jura Mountains and the northern French Pre-Alps during the Last Glacial- Holocene transition: a regional synthesis. Global Planet. Change 30, 85–101.
Maisch, M., 1987. Zur Gletschergeschichte des alpinen Spätglazials: Analyse und Interpretation von Schneegrenzdaten. Geograph. Helv. 42, 63–71.
Marnézy, A., 1999. L'Arc et sa vallée, Anthropisation et géodynamique d'une rivière alpine dans son bassin versant. Joseph Fourier University, Grenoble, France, p. 682. *Ph.D. thesis*.
Martin, L., Blard, P.-H., Balco, G., Lavé, J., Delunel, R., Lifton, N., Laurent, V., 2017. The CREp program and the ICE-D production rate calibrationdatabase: a fully parameterizable and updated online tool to compute cosmic-ray exposure ages. Quat. Geochronol. 38, 25–49.
McCarroll, D., Rijsdijk, K.F., 2003. Deformation styles as a key for interpreting glacial depositional environments. J. Quat. Sci. 18, 473–489.
Miall, A.D., 1978. Fluvial sedimentology. Mem. Can. Soc. Petrol. Geol. 858. Calgary.
Miall, A.D., 1983. Glaciofluvial transport and deposition. In: Eyles, N. (Ed.), Glacial Geology. Pergamon, pp. 168–183.
Miall, A.D., 1996. The Geology of Fluvial Deposits. Springer, New York, p. 582.
Moran, A.P., Ivy-Ochs, S., Schuh, M., Christl, M., Kerschner, H., 2016. Evidence of central Alpine glacier advances during the Younger Dryas early Holocene transition period. Boreas 45, 398–410.
Mulder, T., Alexander, J., 2001. The physical character of subaqueous sedimentary density fows and their deposits. Sedimentology 48, 269–299.
Nemec, W., 1990. Aspects of sediment movement on steep delta slopes. In: Colella, A., Prior, D.B. (Eds.), Coarse-Grained Deltas. Wiley, pp. 29–73.
Nicoud, G., Bourlès, D., Hyppolite, J., Carcaillet, J., Coutterand, S., Paillet, A., 2009. Sur l'âge Dryas récent des moraines frontales du Villaron à Bessans– Savoie – France. Implications dans la lithostratigraphie locale de la déglaciation de la haute vallée de l'Arc (Maurienne – Savoie – France). In: Congrès AFEQ : Rencontre datation : les formations superficielles en domaine continental ; apport des nouvelles méthodes de datation ; Montpellier juin 2009.
Owen, G., 2003. Load structures: gravity-driven sediment mobilization in the shallow subsurface. Geol. Soc. London Spec. Publ. 216, 21–34.
Phillips, E., Lee, J., Burke, H., 2008. Progressive proglacial to subglacial deformation and syntectonic sedimentation at the margins of the Mid-Pleistocene British Ice Sheet: evidence from north Norfolk, UK. Quat. Sci. Rev. 27, 1848–1871.
Porter, S.C., Orombelli, G., 1982. Late-glacial ice advances in the western Italian Alps. Boreas 11, 125–140.
Postma, G., Cruickshank, C., 1988. Sedimentology of a late Weichselian to Holocene terraced fan delta, Varangefjord, northern Norway. In: Nemec, W., Steel, R.J. (Eds.), Fan Deltas: Sedimentology and Tectonic Settings. Blackie and son, pp. 144–157.
Powell, R., 1990. Glacimarine processes at grounding-line fans and their growth to ice-contact deltas. Geol. Soc. London Spec. Publ. 53, 53–73.
Protin, M., Schimmelpfennig, I., Mugnier, J.-L., Ravanel, L., Le Roy, M., Deline, P., Favier, V., Buoncristiani, J.-F., 2019. Climatic reconstruction for the younger Dryas/early holocene transition and the little ice age based on paleo-extents of Argentiere glacier (French Alps). Quat. Sci. Rev. 221, 105863.
Prud'homme, C., Vassallo, R., Crouzet, C., Carcaillet, J., Mugnier, J.-L., Cortés-Aranda, J., 2020. Paired 10Be sampling of polished bedrock and erratic boulders to improve dating of glacial landforms: an example from the Western Alps. Earth Surf. Process. Landforms 45, 1168–1180.
Rajaratnam, N., Subramanyam, S., 1986. Plane turbulent denser wall jets and jumps. J. Hydraul. Res. 24, 281–296.
Rasmussen, S.O., Bigler, M., Blockley, S.P., Blunier, T., Buchardt, S.L., Clausen, H.B., Cvijanovic, I., Dahl-Jensen, D., Johnsen, S.J., Fischer, H., Gkinis, V., Guillevic, M., Hoek, W.Z., Lowe, J.J., Pedro, J.B., Popp, T., Seierstad, I.K., Steffensen, J.P., Winstrup, M., 2014. A stratigraphic framework for abrupt climatic changes during the Last Glacial period based on three synchronized Greenland ice-core records: refining and extending the INTIMATE event stratigraphy. Quat. Sci. Rev. 106, 14–28.
Ravier, E., 2024. Physical characteristics of hydrofracture systems and their fills in glacial sediments. Sediment. Geol. 463, 106593.
Ravier, E., Buoncristiani, J.F., Menzies, J., Guiraud, M., Portier, E., 2015. Clastic injection dynamics during ice front oscillations: a case example from Sólheimajökull (Iceland). Sediment. Geol. 323, 92–109.
Reitner, J.M., Ivy-Ochs, S., Drescher-Schneider, R., Hajdas, I., Linner, M., 2016. Reconsidering the current stratigraphy of the Alpine Lateglacial: implications of the sedimentary and morphological record of the Lienz area (Tyrol/Austria). J. Quat. Sci. 65, 113–144.

Rijsdijk, K., Warren, W., van der Meer, J., 2010. The glacial sequence at Killiney, SE Ireland: terrestrial deglaciation and polyphase glacitectonic deformation. Quat. Sci. Rev. 29, 696–719.
Roattino, T., Crouzet, C., Vassallo, R., Buoncristiani, J.-F., Carcaillet, J., Gribenski, N., Valla, P.G., 2022. Palaeogeographical reconstruction of the western French Alps foreland during the LGM using cosmogenic exposure dating. Quat. Res. (Tokyo) 25, 1–16.
Rohais, S., Eschard, R., Guillocheau, F., 2008. Depositional model and stratigraphic architecture of rift climax Gilbert-type fan deltas (Gulf of Corinth, Greece). Sediment. Geol. 210, 132–145.
Rowan, A.V., Egholm, D.L., Clark, C.D., 2022. Forward modelling of the completeness and preservation of palaeoclimate signals recorded by ice-marginal moraines. Earth Surf. Process. Landforms 47 (9), 2198–2208.
Russell, H.J., Arnott, R.C., 2003. Hydraulic-jump and hyperconcentrated-flow deposits of a glacigenic subaqueous fan: Oak ridges moraines, Southern ontario, Canada. J. Sediment. Res. 73, 887–905.
Russell, A.J., Knudsen, O., 1999. An ice-contact rhythmite (turbidite) succession deposited during the November 1996 catastrophic outburst flood (jökulhlaup), Skeiararjokull, Iceland. Sediment. Geol. 127, 1–10.
Russell, H.J., Sharpe, D., Bajk, A., 2007. Sedimentary signatures of the waterloo moraine, ontario, Canada. In: Hambrey, M., Christoffersen, P., Glasser, N., Hubbard, B. (Eds.), Glacial Processes and Products. Int. Assoc. Sedimentol. Spec. Publ, pp. 85–108.
Rust, B., Romanelli, R., 1975. Late Quaternary Subaqueous Outwash Deposits near Ottawa, Canada, 23. SEPM Spec. Publ., pp. 177–192
Serra, E., Valla, P.G., Gribenski, N., Carcaillet, J., Deline, P., 2022. Post-LGM glacial and geomorphic evolution of the Dora Baltea valley (western Italian Alps). Quat. Sci. Rev. 282, 107446.
Shanmugam, G., 2000. 50 years of the turbidite paradigm (1950s–1990s): deep-water processes and facies models – a critical perspective. Mar. Petrol. Geol. 17, 285–342.
Spagnolo, M., Ribolini, A., 2019. Glacier extent and climate in the maritime Alps during the younger Dryas. Palaeogeogr. Palaeoclimatol. Palaeoecol. 536, 109400.
Tracy, D., Brennand, A., 2000. Deglacial meltwater drainage and glaciodynamics: inferences from Laurentide eskers, Canada. Geomorphology 32, 263–293.
Van Husen, D., 2000. Geological processes during the quaternary. Aust. J. Earth Sci. 92, 135–156.
Van Raden, U.J., Colombaroli, D., Gilli, A., Schwander, J., Bernasconi, S.M., van Leeuwen, J., Eicher, U., 2013. High-resolution late-glacial chronology for the Gerzensee lake record (Switzerland): δ18O correlation between a Gerzensee-stack and NGRIP. Palaeogeogr. Palaeoclimatol. Palaeoecol. 391, 13–24.
Von Grafenstein, U., Erlenkeuser, H., Brauer, A., Jouzel, J., Johnsen, S.J., 1999. A mid-European decadal isotope-climate record from 15.500 to 5000 years B.P. Science 284, 1654–1657.
Wisemann, J., Hornung, J.J., Meinsen, J., Asprion, U., Polom, U., Brandes, C., Burmann, M., Weber, C., 2009. Anatomy of a subaqueous ice-contact fan and delta complex, Middle Pleistocene, North-west Germany. Sedimentology 56, 1041–1076.